The Magnitude of Exhumation in the Kidson Sub-basin, Western Australia, using Thermal and Compaction Techniques

George Marfo
UNSW Sydney
Patrick Makuluni
UNSW Sydney
Stuart Clark (stuart.clark@unsw.edu.au)
UNSW Sydney https://orcid.org/0000-0002-0495-670X

Research Article

Keywords: Apatite Fission Track, Vitrinite Reflectance, Compaction, Exhumation, Canning Basin, Geological Storage, Maturation

Posted Date: July 7th, 2022

DOI: https://doi.org/10.21203/rs.3.rs-1161714/v2

The Magnitude of Exhumation in the Kidson Sub-basin, Western Australia, using Thermal and Compaction Techniques

George Marfo[1], Patrick Makuluni[1], Stuart Clark[1,*]

[1]University of New South Wales Sydney, Kensington, NSW, 2052, Australia.

***Corresponding Author:** *stuart.clark@unsw.edu.au*

Abstract

The Kidson Sub-basin which forms the largest tectonic province of the Canning Basin has a high potential for Uranium, sediment-hosted base metals, conventional and unconventional hydrocarbons. The basin has undergone major tectonic events since its formation in the Early Ordovician involving several inversion episodes resulting in extensive exhumation in the basin. The magnitude, timing and distribution of exhumation associated with these inversion episodes are poorly studied due to sparse data in the area. In this study, we integrate recently acquired seismic data with existing well data, combining for the first time thermal and compaction techniques to constrain the magnitude and distribution of exhumation associated with these major inversion episodes.

Our results indicate that 300 to 500 m of exhumation occurred during the middle Silurian to Early Devonian inversion episode or Prices Creek Compression, 500 to 750 m of exhumation occurred during the middle Carboniferous inversion episode or Meda Transpression and 800 to 1200 m of exhumation occurred during the Late Triassic to Early Jurassic inversion episode or Fitzroy Transpression. Data from apatite fission-track analysis put temporal constraints on the timing of this exhumation and indicate that cooling from maximum post-depositional temperatures within the Kidson Sub-basin occurred in the Late Triassic to Early Jurassic. This imply that a paleothermal maximum was reached within the Kidson Sub-basin during the Early Triassic extension episode, prior to the Fitzroy Transpression. During this period, we also detect that the sediments were affected by a slight increase in basal heat flow associated with the rifting event.

Results illustrate that during each of these inversion events, higher amounts of exhumation affected the Kidson Sub-basin than previously thought. The results from this study also demonstrate two dominant factors controlling the spatial and temporal distribution of exhumation in the Kidson Sub-basin. We suggest that the spatial distribution of exhumation in the sub-basin during each inversion episode was dominantly controlled by variation in rheology (strength) of inherited basement units, whilst the temporal distribution of exhumation was dominantly controlled by variation in the magnitude of compressive stress.

1. Introduction

The Kidson Sub-basin is a part of the onshore Canning Basin in Western Australia (Fig. 1) and has a potential for energy and CO_2 storage as well as conventional and unconventional gas and minerals. While conventional hydrocarbons form the major energy resource produced in the Canning Basin, it is estimated to have the largest unconventional shale gas potential in Australia and 8th largest shale gas potential in the world (Geoscience Australia, 2020; U.S.A Energy Information Administration, 2013, 2011; Western Australia Department of Mines and Petroleum, 2021). The Kidson Sub-basin also contains the largest halite formation in Australia (Hashimoto et al., 2018), one a the most cost-effective methods for underground hydrogen storage (Lord et al., 2014). The Sub-basin also has significant mineral resource prospectivity, such as for Uranium (Botten, 1984) and sediment-hosted base metals (McCracken et al., 1997; Passmore and Towner, 1987; Ringrose, 1984; Veamcombe et al., 1995).

The Kidson Sub-basin formed in the Early Ordovician (~ 480 Ma) and has since undergone three major extensional phases, separated by three major inversion episodes (Hashimoto et al., 2018; Kennard et al., 1994a; Shaw et al., 1994). The inversion episodes are associated with extensive exhumation and have impacted fluid migration, salt dissolution, brine migration and mineralisation in the Canning Basin overall (Hashimoto et al., 2018; Yule and Daniell, 2019). Exhumation studies, therefore, have great implications on understanding the evolution of the Kidson Sub-basin, as well as its hydrocarbon and mineral potential.

Exhumation is the process of removing overburden from a basin or terrane when the rocks are vertically displaced (Corcoran and Doré, 2005; Malusa and Fitzgerald, 2019). Exhumation occurs in a wide variety of geological settings in response to epeirogeny and tectonic processes and as such can be used to study basin evolutionary processes (Gallagher, 2012) and hydrocarbon prospectivity (Corcoran and Doré, 2005; Dore´ et al., 2002; Jensen and Schmidt, 1993). Additionally, exhumation has important significance on halite dissolution and brine migration and mineralisation of basins with salt deposits, influencing the formation and preservation, as well as spatial and temporal distribution of sediment-hosted mineral deposits (Cox et al., 2003; Kesler and Wilkinson, 2006). Thus, exhumation studies have great implication on the tectonic evolution and energy potential of a basin.

As a result of this potential, the Kidson Sub-basin has been the focus of new acquisition of seismic and well data in the area. These new data sets includes an 872 km 2D seismic line across the Kidson Sub-basin, acquired in 2018 and the Barnicarndy-1 stratigraphic well, drilled in 2019 (Geoscience Australia, 2020; Southby et al., 2019). The acquisition of these datasets has led to new understandings of the salt formations in the Kidson Sub-basin, which are the result of tectonic uplift and associated change of the depositional environment from open marine to restricted marine conditions in the Ordovician (Zhan, 2019). Extensive erosional unconformities were also observed on seismic line 18GA-KB1 and have been interpreted to be the result of exhumation during major basin inversion episodes (Southby et al., 2019). Prior to this new acquisition, there have been exhumation studies based on wells in the broader Canning Basin, such as that of Duddy et al. (2003, 2006) and Green (2014) that studied the thermal history reconstruction of the Canning Basin. These studies found that the paleo-thermal maximum in the Canning Basin was likely attained between the Late Triassic to Early Jurassic. Exhumation has therefore strongly affected the geological evolution of the Canning Basin and

by implication the Kidson Sub-basin too. These studies provide evidence on the existence of uplift and some constraints on the timing, but a detailed study of the exhumation of the Kidson Sub-basin remains to be carried out based on the new data.

In this study we integrate the newly acquired seismic data with existing wells (13 wells) to quantify the magnitude of exhumation in the Kidson Sub-basin (Fig. 1). This includes three wells located on the adjacent Munro Arch and Ryan shelf (Fig. 1). The study involved a detailed interpretation of the newly acquired seismic line (Kidson seismic survey 18GA-KB1-60km), highlighting exhumation features within the basin. We employed two methods of analysis to better constrain the basin evolution from the available data. Firstly, a thermal study involving analysis of Vitrinite Reflectance (VR) data and a comparison of results from a compaction technique using porosity data from core and well logs. These methods are discussed in more detail below. Results from both methods are independent and complementary and were used to constrain the timing, magnitude, and the distribution of exhumation during major inversion episodes in the Kidson Sub-basin. In the next section, we describe the geological setting of the Kidson Sub-basin.

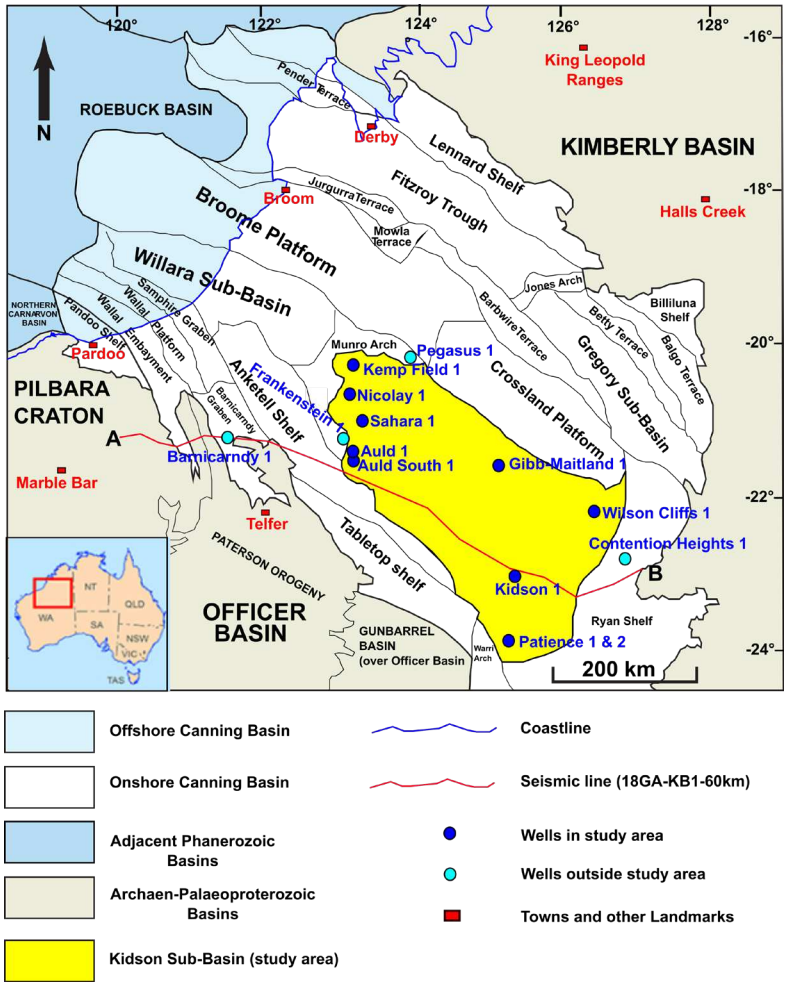

Figure 1. Location map of the Canning Basin showing tectonic provinces (including Kidson Sub-basin) as well as seismic line 18GA-KB1-60km and wells used for this study (Modified from Carlsen and Ghori, 2005). Inset (bottom left corner) is the map of Australia showing the

approximate location of the Canning Basin (red box) (modified from Bradshaw et al., 2012). The Canning Basin located in Western Australia is divided into onshore and offshore component. The onshore Canning component developed as an intra-cratonic basin during the Early Ordovician and has undergone a prolonged period of extensional and compressional deformation which has structured the basin into several tectonic features. Wells in the Kidson Sub-basin used in this study include Kidson-1, Sahara-1, Wilson Cliffs-1, Frankenstein-1, Kemp Field-1, Nicolay-1, Patience-1, and Contention Heights-1.

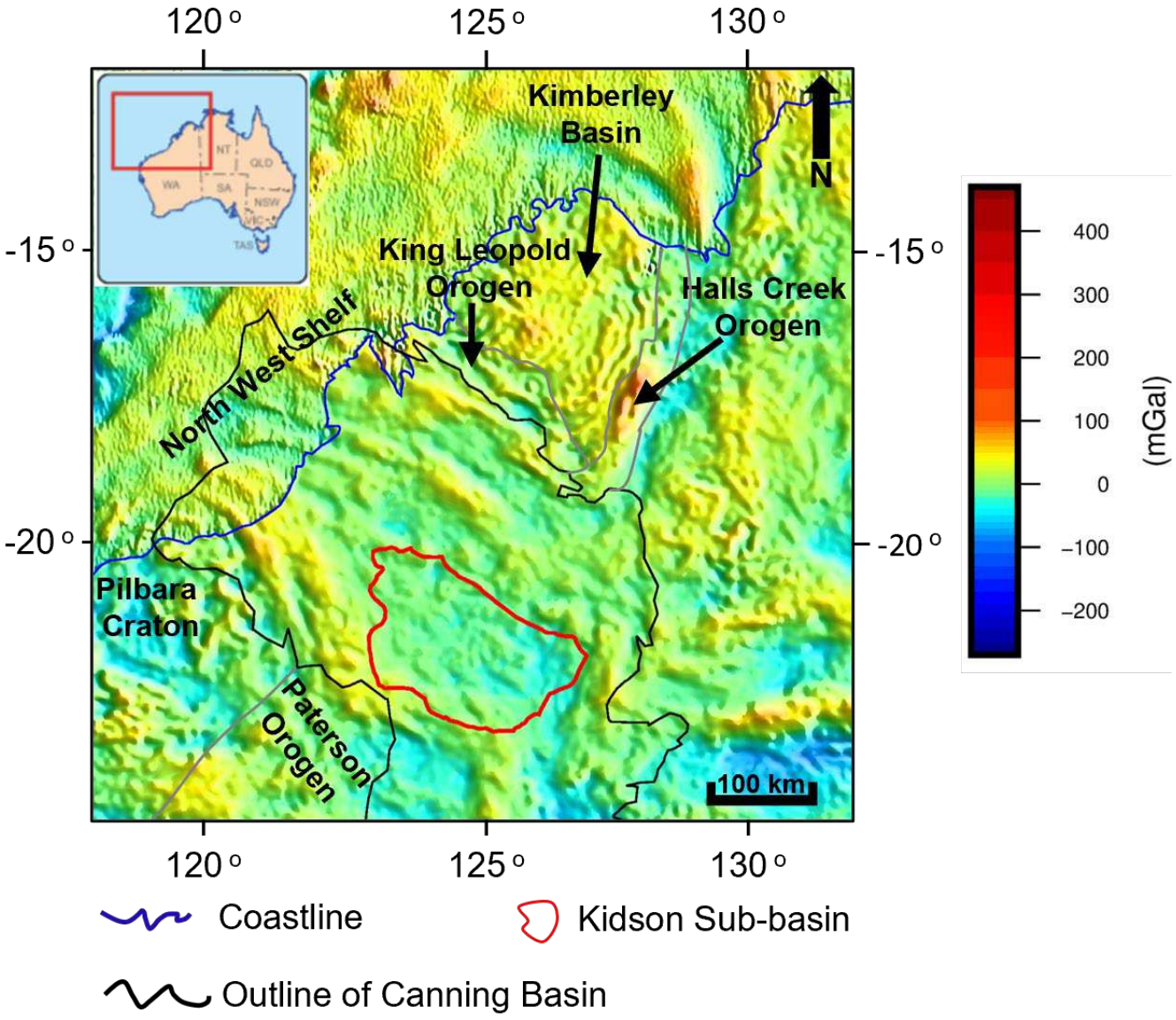

Figure 2. Free Air gravity anomaly map of the Canning Basin (including Kidson Sub-basin) and surrounding areas. Insert (top left corner) is the map of Australia showing the approximate location of the Canning Basin (red box) (modified from Bradshaw et al., 2012). The onshore Canning Basin was initiated between two sets of cratonic blocks: the Halls Creek and King

Leopold orogens to the northeast; and the Paterson Orogen and Pilbara Craton to the southwest.

2. Geological setting and evolution

The Canning Basin is the largest sedimentary basin in Western Australia covering an approximate area of 530,000 km². The basin is divided into an onshore portion described to be an intra-cratonic system and an offshore portion which is described to be part of a passive margin system (Bradshaw et al., 2012; Carlsen and Ghori, 2005; Forman and Wales, 1981; Western Australia Department of Mines and Petroleum, 2021). The onshore intra-cratonic system is constituted by two major northwest to southeast trending depositional centres (Fig. 1 and 2), which are separated from each other by basement platforms and surrounded by shelves and terraces (Fig. 1). These depocenters comprise the (i) Fitzroy Trough–Gregory Sub-basin complex located within the northern part of the basin and (ii) Willara–Kidson Sub-basin complex located within the southern portion of the basin (Fig. 1; Hashimoto et al., 2018). The Kidson Sub-basin is the largest amongst all the depocenters and tectonic provinces in the basin and occupies the south-eastern corner of the basin (Fig. 1).

The onshore Canning Basin, which hosts the Kidson Sub-basin, is an intra-cratonic rift basin that developed in the Early Ordovician (Bradshaw et al., 2012; Carlsen and Ghori, 2005; Forman and Wales, 1981; Hashimoto et al., 2018; Shaw et al., 1994). After the basin's formation, the onshore Canning Basin underwent several major basin-wide active tectonic periods involving extension, subsidence, inversion and exhumation (uplift and erosion) which resulted in the development of the individual depocenters and tectonic features in the basin (Hashimoto et al., 2018; Shaw et al., 1994). Compared to the northern sub-basins, the southern sub-basins (Kidson and Willara) are less deformed characterised by the lack of significant fault block movements (Western Australia Department of Mines and Petroleum, 2021, 2014). The Kidson Sub-basin together with the other sub-basins within the Canning Basin are dominated by Ordovician to Permian sediments with minor or no Mesozoic and Cenozoic sediments. Sediments within the Kidson Sub-basin are generally thinner with total sediment thickness of 5 km compared to the thicker sediments of more than 15 km in the northern parts of the Canning Basin (Kennard et al., 1994a). The sediments within the Kidson Sub-basin were deposited within a wide variety of depositional environments ranging from marine to non-marine comprising marine shelf, carbonate reef, paralic, fluvial, fluvio-deltaic, aeolian and evaporitic sediments (Cadman et al., 1993; Forman and Wales, 1981). The evolution of the Kidson Sub-basin is linked to the overall evolution of the Canning Basin. A complete tectonic and sequence stratigraphic evolution of the Kidson Sub-basin is summarised in Fig. 3 and presented in the next section.

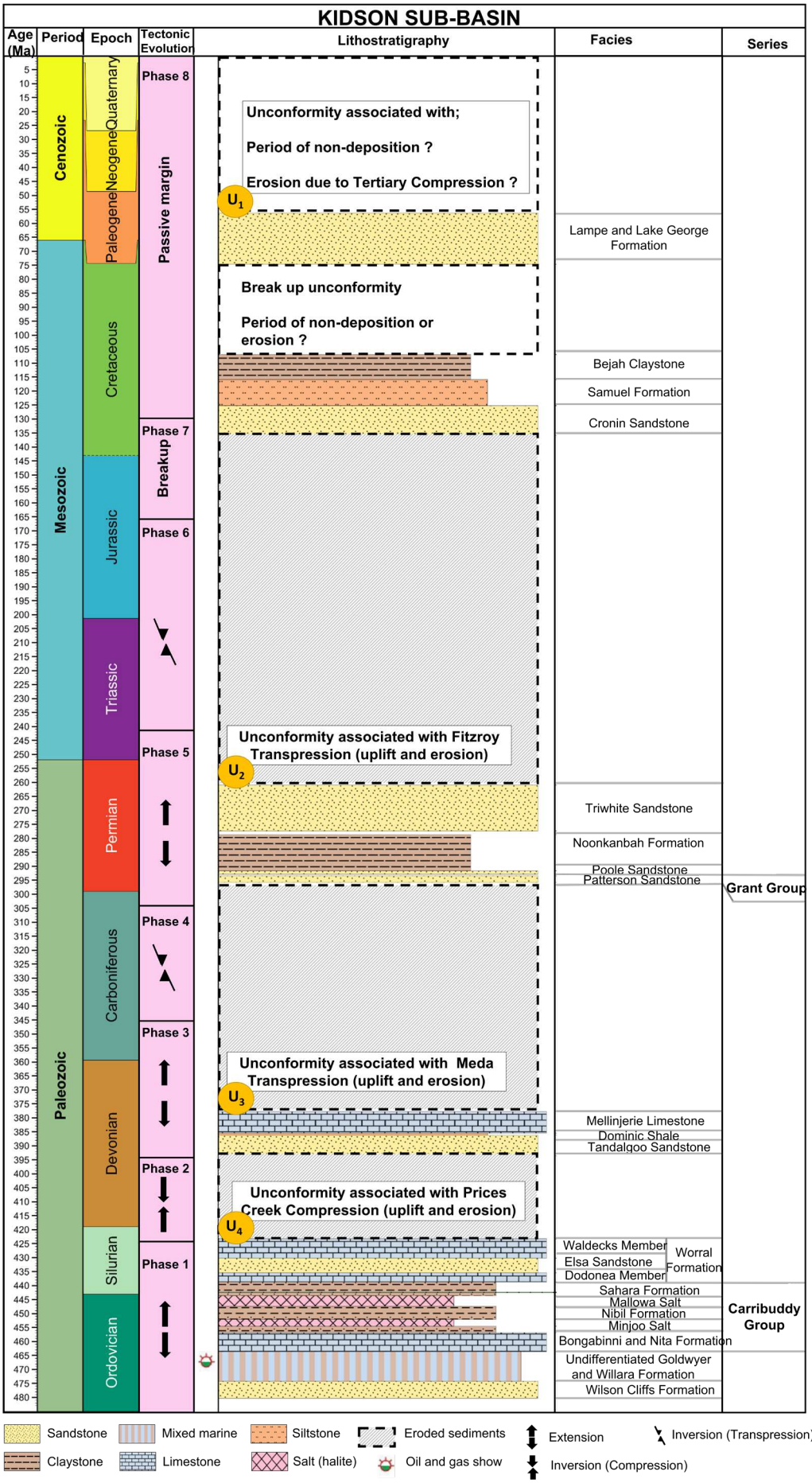
KIDSON SUB-BASIN
Age (Ma)
Period
Epoch
Tectonic Evolution
Lithostratigraphy
Facies
Series
Cenozoic
Mesozoic
Paleozoic
Quaternary
Neogene
Paleogene
Cretaceous
Jurassic
Triassic
Permian
Carboniferous
Devonian
Silurian
Ordovician
Phase 8
Passive margin
Phase 7
Breakup
Phase 6
Phase 5
Phase 4
Phase 3
Phase 2
Phase 1
Unconformity associated with;
Period of non-deposition ?
Erosion due to Tertiary Compression ?
U1
Break up unconformity
Period of non-deposition or erosion ?
Unconformity associated with Fitzroy Transpression (uplift and erosion)
U2
Unconformity associated with Meda Transpression (uplift and erosion)
U3
Unconformity associated with Prices Creek Compression (uplift and erosion)
U4
Lampe and Lake George Formation
Bejah Claystone
Samuel Formation
Cronin Sandstone
Triwhite Sandstone
Noonkanbah Formation
Poole Sandstone
Patterson Sandstone
Grant Group
Mellinjerie Limestone
Dominic Shale
Tandalgoo Sandstone
Waldecks Member
Elsa Sandstone
Dodonea Member
Worral Formation
Sahara Formation
Mallowa Salt
Nibil Formation
Minjoo Salt
Bongabinni and Nita Formation
Carribuddy Group
Undifferentiated Goldwyer and Willara Formation
Wilson Cliffs Formation
Sandstone
Claystone
Mixed marine
Limestone
Siltstone
Salt (halite)
Eroded sediments
Oil and gas show
Extension
Inversion (Compression)
Inversion (Transpression)

Figure 3. Generalised litho-stratigraphy of the Kidson Sub-basin showing the evolution of the basin as well as stratigraphic relationships between formations and major unconformities [created using timescale creator with reference from Command Petroleum NL (1989); Forman and Wales (1981); Hashimoto et al., (2018); Shaw et al. (1994)]. The Kidson Sub-*basin has undergone three major extensional phases separated from each other by three major compressional/transpression episodes. The extensional episodes resulted in deposition of major sedimentary sequences whilst the episodes of basin inversion resulted in* exhumation*. Unconformity, U_1 is associated with either a period of non-deposition or minor* exhumation *episode during the* Cenozoic*. Unconformities, U_2, U_3 and U_4 are associated with major exhumation periods that affected the Kidson* Sub-*basin and* are *the focus of this study.*

Phase 1: Early Ordovician – middle Silurian (500 – 420 Ma)

Multiple extensional events affected Western, Central, Eastern and Northern Australia during the Early Ordovician associated with the breakup of microcontinents from the northeastern Gondwanan supercontinent (Johnson et al., 2017). In western Australia, these extensional activities led to the initiation of the onshore Canning Basin as an intra-cratonic rift basin between two main sets of cratonic blocks; the Halls Creek and King Leopold orogens to the northeast and the Paterson Orogen and Pilbara Craton to the southwest (Fig. 2; Hashimoto et al., 2018; Hocking et al., 1994). This early extension that initiated the basin has been named the Samphire Marsh Extensional Movement (Shaw et al., 1994). During this extension and early basin development, the Kidson and Willara Sub-basins developed as relatively broader and shallower graben and half-graben depocenters (Hashimoto et al., 2018). On the other hand, the northern depocenters (Fitzroy Trough and Gregory Sub-basin) developed as narrow and deeper graben and half-graben structures. Anatomically, the graben and half graben structures of the Kidson Sub-basin have been described as relay-style accommodation zones that developed between overlapping fault blocks (Shaw et al., 1994). In comparison with other parts of the basin, faulting was less prevalent in the Kidson Sub-basin, Broom platform, and Crossland platform (Hashimoto et al., 2018). Rather, these areas were dominated by intra-cratonic sag during this period (Hashimoto et al., 2018).

Extension was accompanied by Subsidence of more than 1.5 km across the major depocenters in the Canning Basin including the Kidson and Willara Sub-basins and the Fitzroy Trough (Shaw et al., 1994). Subsidence at this time was strongly influenced by basement heterogeneities and initial basin tectonics (Shaw et al., 1994). Tectonic provinces that experienced slower Subsidence such as the Kidson Sub-basin seem to strongly correlate with more stable and older basement areas (Hashimoto et al., 2018). Associated extension-related subsidence led to the formation of transgressive environments and the deposition of thick sedimentary sequences over the basement during the Early Ordovician to late Silurian period (Fig. 3; Kennard et al., 1994a; Parra-Garcia et al., 2014). The sequence is about 3 km thick over much of the Canning Basin, with thicknesses up to 5 km within the Kidson Sub-basin (Hashimoto et al., 2018). The lower part of this sequence comprises shallow to deep marine mixed siliciclastic and carbonate successions (mudstone, dolostone, limestone and sandstone) of the Wilson Cliffs, Goldwyer, Willara, Bongabinni and Nita formations with the Goldwyer

Formation marking the maximum flooding surface within the basin (Fig. 3; Kennard et al., 1994a; Parra-Garcia et al., 2014).

During the Late Ordovician to early Silurian, depositional environment changed from open marine to restricted evaporitic conditions across much of the basin (Parra-Garcia et al., 2014; Zhan, 2019). This change is strongly correlated to a combination of regression and tectonic uplift related to the early episodes of the Alice Spring Orogeny (Zhan, 2019). The restricted evaporitic environments were synchronous with arid climatic conditions and led to the deposition of thick salt sequences of the Minjoo and Mallowa salt of the Curibbudy Group in the southern Kidson and Willara sub-basins (Fig. 3; Forman et al., 1981; Parra-Garcia et al., 2014; Zhan, 2019). Particularly, the Mallowa salt is up to 800 m thick within the central Kidson Sub-basin and is considered as the most extensive halite deposit in Australia (Hashimoto et al., 2018).

Phase 2: Late Silurian to Early Devonian (420 – 400 Ma)

The late Silurian to Early Devonian period was characterised by a change from an initial extension to a compressional tectonic regime correlated to major peak episodes of the Alice Springs Orogeny that affected much of central Australia (Shaw et al., 1994). This compressional event (termed the Prices Creek Compression) resulted in extensive tilting, folding, uplifting, onlap and erosion of sedimentary units resulting in an angular unconformity on top of the Ordovician to Silurian sedimentary sequence over much of the Canning Basin (Fig. 3; Hashimoto et al., 2018; Parra-Garcia et al., 2014; Shaw et al., 1994). This deformation is also suggested to have initiated extensive salt dissolution and brine migration within the Canning Basin (Hashimoto et al., 2018).

Phase 3: Early Devonian to early Carboniferous (400 – 345 Ma)

Extension resumed from the Late Devonian to early Carboniferous period (Fig. 3). The main rifting (extension) phase was preceded by a pre-rift sag (Tandalgoo sag) phase in the Early to Middle Devonian and this sag-related basin subsidence period was attributed to extension in the lower crust with no major extension in the upper Crust (Shaw et al., 1994). Aeolian, fluvial, playa and marginal marine sedimentary facies composing the Millinjerie Limestone, Tandalgoo Sandstone and Dominic Shale were deposited at this time (Fig. 3; Hashimoto et al., 2018; Kennard et al., 1994a). The main extensional event (termed Pillara Extensional Movement) started during the Late Devonian with the development of normal faults and the reactivation of older faults, especially the Beagle Bay-Pinnacle and Fenton Fault Systems and the formation of accommodation zones between fault segments (Hashimoto et al., 2018). Following this extension, and associated subsidence, widespread transgression developed across the entire Canning Basin (Forman and Wales, 1981). Fluvio-deltaic complexes, hypersaline lagoonal deposits, carbonate reef complexes and mixed carbonate-siliclastic ramps were deposited composing the Cadjebut Formation, Fairfield Formation, Anderson Formation, Pillara and Nullara sequences (Cadman et al., 1993; Kennard et al., 1994a; Parra-Garcia et al., 2014). These sequences are not observed in the Kidson Sub-basin and this may be due to their subsequent erosion. Varying rates of tectonic subsidence controlled and led to the deposition and variation in the thickness of the Devonian to early carboniferous sequences across the basin

(Parra-Garcia et al., 2014). These sequences range in thickness from thin (between 20 and 300 m thick) on the Broome Platform, to very thick (between 6-15 km) on the Fitzroy Trough (Hashimoto et al., 2018).

Phase 4: Middle Carboniferous (345 – 320 Ma)

The ongoing extension was disrupted by basin inversion associated with transpressional tectonics during the middle to late Carboniferous period (Shaw et al., 1994). The cause of this inversion episode is suggested to be the far-field effect of Laurasia-Gondwana collision (Fig. 3; Hashimoto et al., 2018). The inversion event, ended the Meda Transpressional Movement, resulting in mild folding, extensive uplift and erosion, and reactivation of extensional faults producing flower and pop-up structures, which are evident in most part of the basin (Shaw et al., 1994). The erosion of part of the Devonian and carboniferous sequence resulted in a major unconformity at the base of the Lower Grant Group, which laterally extend across the entire basin (Forman and Wales, 1981).

Phase 5: Late Carboniferous to Early Triassic (320 – 240 Ma)

During the late Carboniferous to Triassic period, north to northeast oriented transpressional tectonism renewed across the basin resulting in a tilted orientation of the Canning Basin in comparison to ongoing rifting along the Gondwana Margin (Fig. 3; Hashimoto et al., 2018; Parra-Garcia et al., 2014). This event has been termed, Point Moody Extension (Shaw et al., 1994). Associated tectonic related subsidence was widespread across the Canning Basin and the deposition of transgressive and regressive sequences included glacial, fluvio-deltaic to marine deposits of the Upper Grant Group (Fig. 3; Cadman et al., 1993; Forman and Wales, 1981; Kennard et al., 1994a). The main rifting phase at this period was succeeded by a post-rift thermal sag phase initiating a transgressive-regressive cycle and resulting in the deposition of the Noonkanbah Formation, Poole Sandstone and Liveringa Group that reach thicknesses of more than 700 m over much of the Kidson Sub-basin (Fig. 3; Cadman et al., 1993; Shaw et al., 1994).

Phase 6: Late Triassic – Early Jurassic (240 – 165 Ma)

During the Late Triassic to Early Jurassic the entire Canning Basin experienced an inversion episode associated with dextral transpressional movements that affected basement blocks at the margins of the basin, especially the Fitzroy Trough (Fig. 3; Hashimoto et al., 2018; Shaw et al., 1994). This inversion episode, termed Fitzroy Transpressional Movement, resulted in extensive folding, reactivation of extensional faults, deformation and remobilization of salt deposits and intense uplift and erosion of Permian-Triassic strata across the entire basin (Hashimoto et al., 2018; Shaw et al., 1994). This event is considered to be a crucial tectonic event that affected the entire petroleum system of the Canning Basin including cooling of source rocks, trap formation and breaching and affecting seal integrity (Zhan and Mory, 2013). The large synclines and anticlines observed in the centre of the Fitzroy Trough and the regional unconformity at the base of the Jurassic sequence are attributed to this inversion episode (Shaw et al., 1994). This compressional deformation was accompanied by the emplacement of isolated intrusive bodies in the Fitzroy Trough and Lennard Shelf (Hashimoto et al., 2018; Reeckmann and Mebberson, 1984).

Phase 7 and Phase 8: Middle Jurassic – Cenozoic

During the Middle Jurassic, northwest to southeast oriented extension that led to the final Gondwana breakup was initiated in the Argo Abyssal Plain, in the adjacent northern Carnarvon Basin (Shaw et al., 1994). Associated Subsidence related to this extension resulted in the establishment of aeolian, fluvial and delta plain environmental conditions into the onshore Canning Basin and the deposition of conglomerate, coal, mudstone and sandstone over the offshore Canning basin (Cadman et al., 1993; Forman and Wales, 1981; Parra-Garcia et al., 2014). Similar sedimentary sequences were deposited onto the onshore Canning Basin during the Early Cretaceous period following the breakup of Greater India from Australia and the development of the northwestern Australian passive margin (Betts et al., 2002; Hashimoto et al., 2018; Kennard et al., 1994a). The present-day onshore Canning Basin has been terrestrial since the middle Cretaceous time except for the occasional flooding of marine waters along the present-day coast (Johnson et al., 2017).

During the Oligocene to Miocene time, the northern margin of the Australian plate collided with southeast Asian microplates resulting in extensive deformation involving reactivation of Paleozoic to Mesozoic faults and basin inversion across the North West Shelf (Keep et al., 2007). This appears not to have affected the adjoining onshore Canning Basin significantly (Hashimoto et al., 2018; Keep et al., 2007), however, mild uplift and erosion across the onshore Canning Basin are attributed to this Cenozoic event (Shaw et al., 1994).

3. Data sets and Methods

3.1. Data sets

This study integrates seismic reflection data and well data obtained for the Kidson Sub-basin. The location of seismic and well data used for this study is shown in Fig. 1. Additionally, thermal history analysis (using AFTA data) and burial history modelling obtained from other independent studies (Duddy et al., 2006, 2003; Ghori, 2013; Green, 2014) have been integrated with this study. The seismic data (Survey 18GA-KB1-60km) is a relatively new data acquired by Geoscience Australia in 2018. It is a Pre-stack Depth Migrated 2D seismic line with a sampling rate of 2 ms and 150-fold. The seismic line covers a total length of 872 km and images major tectonic units within the Canning Basin including the Wallal Embayment, Barnicandy Graben, Anketell Shelf, Kidson Sub-basin and Ryan Shelf (Fig. 1). The Kidson Sub-basin is the main Sub-division imaged by the seismic survey.

Well data used in this study includes well-logs (interval transit time from sonic log, density, gamma ray), core porosity, litho-stratigraphic data, vitrinite reflectance data, well completion reports, and surface and bottom hole temperature measurements. These are open file data obtained from the Western Australia Petroleum and Geothermal Information Management System (WAPIMS). Stratigraphic information and well log data are shown in Fig. 4. Vitrinite reflectance data and present-day temperature measurements are shown in Table 1 and Table 2 respectively. The number of sample runs (N) used to determine the maximum mean VR for each sample was obtained for only two wells. For Kidson-1, N ranged from 9 to 28; For Contention Heights-1, N ranged from 9 to 11. Where VR data were not available, especially

withing pre-Silurian sediments, Graptolite Reflectance data were converted to equivalent VR using Eqn. 1 after *Luo et al. (2020)*

$$VReq = (RGrapt\,max * 0.515) + 0.506 \qquad (1)$$

The compressional sonic velocity (interval transit time, Δt) was used as a proxy for porosity because interval transit times are directly related to porosity which is a direct effect of compaction (Hillis, 1995; Tassone et al., 2014). This is because, contrary to density logs that measure bulk porosity of a sedimentary unit, sonic waves do not generally pass through void spaces and open fractures and the associated interval transit time therefore measures the primary porosity of the sedimentary unit (Tassone et al., 2014). Sonic velocities from shale lithologies are widely used since shales exhibit the most simple velocity-depth trend (Hillis, 1995; Licciardi et al., 2020; Magara, 1980; Tassone et al., 2014). Sandstone lithologies also show a consistent porosity-depth relationship and have been employed extensively in basin analysis (Allen and Allen, 2013; Corcoran and Doré, 2005). Thus, in this study, we employ compressional sonic velocity data obtained from both sandstone and shale lithologies, and core porosity data obtained from sandstone lithologies to estimate the magnitude of exhumation across the Kidson Sub-basin. Within sandstone intervals, core porosity data provided additional constraint to log porosity data. Particularly for the Kidson Sub-basin, one advantage of using log porosity from sandstone intervals is that most shale intervals are mixed lithologies, making it difficult to isolate clean shale zones for analysis. However, clean sandstone intervals were readily available from the log data (Fig. 4).

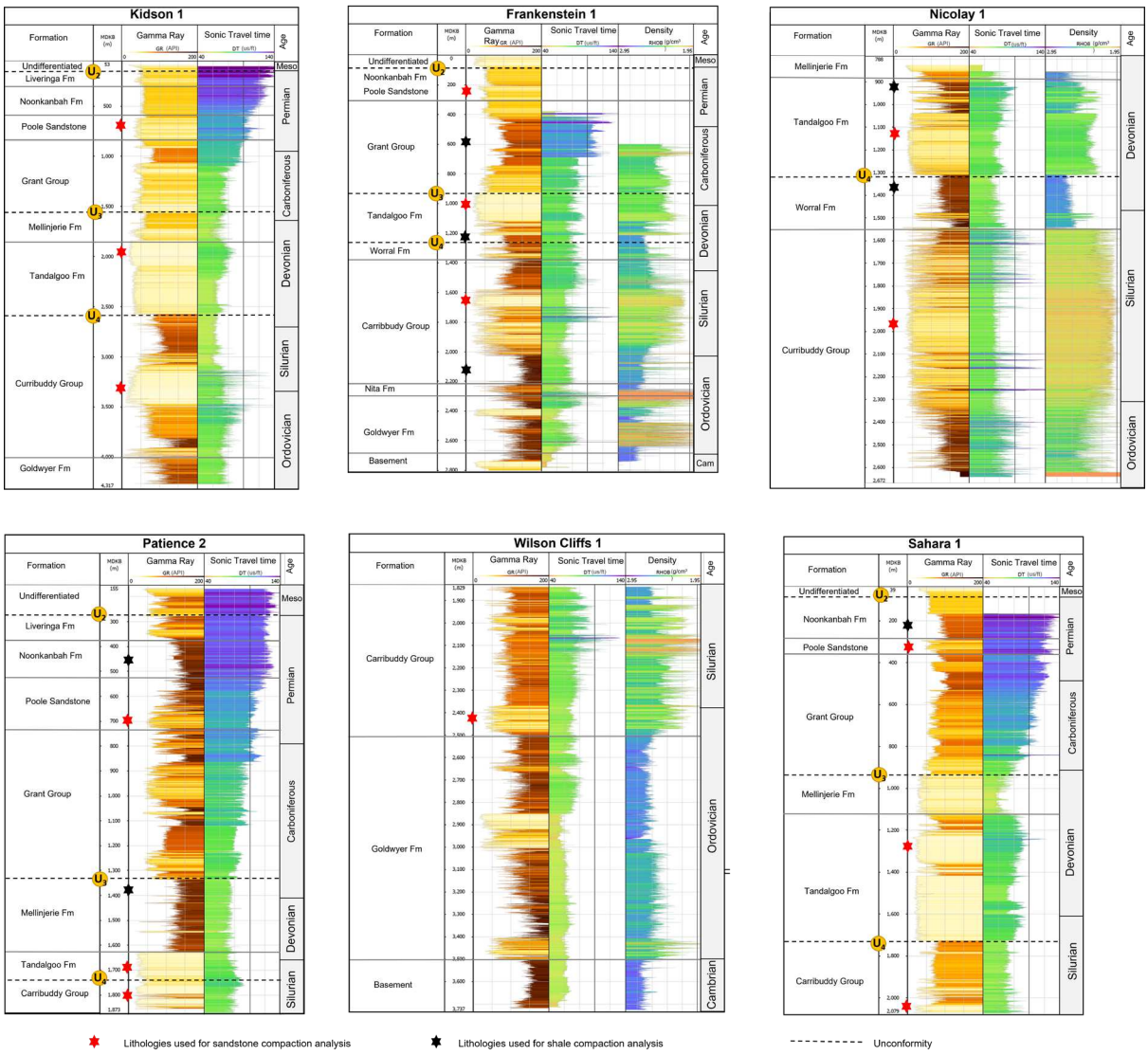

Figure 4. Well log and stratigraphic data used for this study. Stratigraphic information from well data is used to identify position and timing of unconformities at each well location Gamma ray and density logs were combined with core description and other stratigraphic data from well completion reports to delineate sandstone and shale lithologies for analysis. Sandstone units used for analysis were obtained from the Poole Formation (to constrain exhumation at unconformity U_2), Tandalgoo Formation (to constrain exhumation at unconformity U_3) and Carribuddy Group (to constrain exhumation at unconformity U_3). U_1, U_2, and U_3 correspond to erosional unconformities (exhumation) associated with the Fitzroy Transpression, the Meda Transpression and the Prices Creek Compression, respectively.

Table 1. Raw Vitrinite Reflectance data and equivalent maximum paleo-temperatures obtained from wells in the study area. For definitions of Vr and T see the Eqn. 2 and 3.

Well Name	Depth (range) mRT	Vr (Range) %	Paleo-temperature T (°C)	
			Barker and Pawlewicz (1994) [1]	Sweeney and Burnham (1990) [2]
Kidson-1				
	(210.31-213.36	0.41	64	**78**
	265	0.44(0.36-0.51)	69	**84**
	582.16-585.21	0.51(0.41-0.61)	81	**97**
	693	0.47	75	**90**
	707	0.49	78	**94**
	798.57-801.62	0.52	83	**99**
	906.78	0.52	83	**99**
	1022.6	0.54	86	**103**
	1045.46-1048.51	0.54	86	**103**
	1246.63-1249.68	0.55	87	**104**
	1304.54-1307.59	0.55	87	**104**
	1441.70-1444.75	0.59	93	**110**
	1551.4	0.96	132	**154**
	1553	0.53**	84	**101**
	1576	1.08	142	**165**
	4184	2.3	202	**233**
	4365.04-4365.09	2.01*	191	**221**
	4367.5	2.16	197	**227**
	4425.98-4425.99	?2.01*	191	**221**
Frankenstein-1				
	190-200	0.46	72.86	**88**
	500-510	0.50	79.58	**96**
	880-890	0.51	81.18	**97**
	2220.6	0.98*	133.85	**156**
	2339-2342	1.14*	146.05	**170**
	2369-2371	1.21*	150.86	**175**
	2459-2462	1.21*	150.86	**175**
	2600-2603	1.45*	165.45	**191**
	2663-2666	1.43*	164.33	**190**
Nicolay-1				
	2888.3	1.16 *	147	**171**
	2935.3	1.08*	142	**165**
	3003.7	1.21 *	151	**175**
	3043	1.25 *	153	**178**
	3075.5	1.26 *	154	**178**
	3121.2	1.42*	164	**190**
Contention Heights-1				
	107	0.51 (0.39-0.62)	81	**97**
	732	0.6 (0.57-0.62)	94	**112**
	1530	0.83 (0.75-0.93)	121	**141**

Well Name	Depth (range) mRT	Vr (Range) %	Paleo-temperature T (°C)	
			Barker and Pawlewicz (1994) [1]	Sweeney and Burnham (1990) [2]
Patience-2				
	860-870	0.43	67	**82**
	1070-1080	0.44	69	**84**
	1110-1120	0.49	78	**94**
	3048-3051	1.09*	142	**166**
	3081-3084	1.13*	145	**169**
	3153-3156	1.11*	144	**167**
	3246-3249	1.12*	145	**168**
	3453-3459	1.15*	146	**171**
Sahara-1				
	222.5	0.22	13	**22**
	307.5	0.45	71	**86**
	327.6	0.48	76	**92**
	338.3	0.48	76	**92**
	653.8	0.74	111	**131**
	1094.2	0.84	121	**142**
Wilson Cliffs-1				
	347	0.75	112	**132**
	355.092	0.99 (0.52-1.81)	135	**157**
	408	0.52	83	**99**
	411.48	0.56 (0.96-1)	89	**106**
	502.92	0.54 (0.42-0.79)	86	**103**
	494	0.54	86	**103**
	631	0.63	98	**116**
	633.984	0.7 (0.55-1.06)	107	**126**
	1013.9	0.52**	83	**99**
	2133	0.88	125	**147**
	2141.22	0.99 (0.64-1.91)	135	**157**
	2529.84	0.68**	104	**123**
	2530	0.68**	104	**123**
	2588	1.04	139	**162**
	2590.8	1.06 (0.68-1.51)	140	**163**
	2621	0.7**	107	**125**
	2621.28	0.7**	107	**125**
	2680.7	1.35	160	**185**
	2712.72	0.86**	123	**144**
	2713	0.86**	123	**144**
	2780	1.15	147	**171**
	2781.3	1.15 (0.89-1.7)	147	**171**
	2804	0.79**	114	**137**
	2804.16	0.79**	114	**137**
	2958.8	1.94	189	**218**
	3169.92	0.87**	124	**145**
	3170	0.87**	124	**145**
	3185.16	1.23 (0.84-1.67)	152	**177**
	3243	1.26	154	**179**

Well Name	Depth (range) mRT	Vr (Range) %	Paleo-temperature T (°C)	
			Barker and Pawlewicz (1994) [1]	Sweeney and Burnham (1990) [2]
Wilson Cliffs-1				
	3247.645	1.29 (0.89-1.84)	156	**181**
	3282.3	2.61***	213	**244**
	3284.22	2 (1.95-2.48)	191	**220**
	3352.8	1.69	177	**205**
	3352.8	0.84**	121	**142**
	3353	0.84**	121	**142**
	3535.68	0.85**	122	**143**
	3536	0.85**	122	**143**
	3581	2.03	193	**222**
	3618	2.59	212	**243**
	3718	0.89**	126	**148**
	3718.56	0.89**	126	**148**
	3622.55	2.81(2.15-3.58)	219	**251**

Range of VR values are shown in brackets. Mean maximum VR values (Vr) are not in brackets and were used for temperature conversion.

** = equivalent VR calculated from Graptolite reflectance (Eqn. 1)*

*** = Vr (mean maximum VR) values either reported or herein interpreted as cavings or suppressed VR.*

**** = VR values interpreted as possible inherited vitrinite or the result of localised heating from nearby hot fluids or intrusives.*

[1] = Temperature estimates from empirical model (Eqn. 3)

[2] = Temperature estimates from kinetic model (Eqn. 2). These estimates were used for analysis in this study

Table 2. Present-day temperature analysis for wells in the study area.

Well Name	KB (mAMSL)	Ground level (m)	Present-day surface Temp (°C)	Depth-kB (m)	BHT (°C)	Corrected BHT (°C)[1]	Geothermal Gradient °C/km[2]
Nicolay-1							
	287.7	278	23	2635	87.0	104 .0	37.1
				3535	126.0	152.5	

Wilson Cliffs-1						
		24	1005.5	50.6	56.7	
			1908.7	64.4	73.3	
			2387.5	78.9	93.6	28
	445	440	2784.0	84.4	100.5	
			3047.1	96.1	115.1	
			3721.6	120	145	
Frankenstein-1						
	287.27	280.27	2011	78.89	93.6	35.2
			2792	102.2	122.8	
Kidson-1						
			914.7	53.3	60	
		23	2132.4	72.2	85.3	
			2803.2	80	95	
	360	355.1	2840.7	76.7	90.9	31.8
			3144.3	90	107.5	
			3833.8	108.9	131.1	
			4429.4	123.3	149.1	
Sahara-1						
	269.4	264.6	1240.5	66.7	78.4	44.3
			2077	78.9	93.6	
Contention Heights-1						
	423	418	561	47	52.4	31.0
			1672	66	77.5	
Patience-2						
	419	410	2917	83.33	99.1	
			3231	99.44	119.3	29.3
			3779.6	107.22	129	

[1]*Bottom Hole Temperature (BHT) measurements were used since drill-stem tests (DSTs) temperatures were not available. BHT measurements were corrected following* Duddy et al. (2003) and Duddy and Erout (2001). *For measured BHT < 66^{0}C, correction was made by increasing the measured BHT by 20% of the difference between the BHT and surface temperature, and for measured BHT, correction was made by increasing the measured BHT by 25% of the difference between the BHT and surface temperature.*

[2] = *Present-day geothermal gradients*

3.2. Methodology

As the first step, seismic interpretation was conducted to identify and establish features associated with exhumation in the Kidson Sub-basin. Seismic interpretation was followed with estimating the amount of exhumation at the individual well location. The amount of exhumation in sedimentary basins are estimated using one of four main frames of reference: tectonic-based, thermal-based, compaction-based and stratigraphic-based (Corcoran and Doré, 2005). In this study, the thermal and compaction-based techniques were both employed to estimate the magnitude of exhumation in the Kidson Sub-basin. Combining these two methods

offers the advantage of providing independent results that can be used to constrain exhumation magnitudes in basins (Johnson et al., 2017; Makuluni et al., 2021). The methods are described in detail in the following sections.

3.2.1. Seismic Interpretation

Seismic interpretation involved a detailed interpretation of line 18GA-KB1-60km (pre-stack depth migrated) across the Kidson Sub-basin (see Fig. 1 and 7 for location and interpretation of seismic line). Interpretation was done using DUG Insight. Check shot data or density and neutron logs from boreholes were used to generate synthetic seismograms, which were used to tie the well (borehole) to seismic data. Several horizons, corresponding to formation tops in the borehole were then selected and mapped across the seismic line. In this work, the main horizons that were selected and mapped corresponds to formation tops as well as erosional unconformities associated with exhumation. Structural features such as faults and folds were also identified and mapped out. Seismic interpretation was conducted mainly to identify lithological, chronostratigraphic, and seismic stratigraphy as well as the location, extent, and approximate timing of erosional unconformities associated with exhumation within the Kidson Sub-basin. The amount of exhumation at the various unconformities was estimated.

3.2.2. Thermal-based technique for estimating the amount of exhumation

The general principle for the use of paleo-thermal data (thermal-based method) for exhumation analysis is that rocks are heated when buried but cool when exhumed provided that the paleo-geothermal gradient did not vary through time (Bray et al., 1992; Malusa and Fitzgerald, 2019). Thermal indicators such as vitrinite reflectance (VR) or Apatite Fission Track analysis (AFTA) provide information on the temperature a rock unit has experienced in the geologic past (Green et al., 2002). In the case of VR, the measured reflectance is an irreversible indicator of the maximum paleo-temperatures reached in the past before the start of a cooling episode that is usually caused by exhumation (Allen and Allen, 2013; Bray et al., 1992; Gallagher, 2012; Green et al., 2002). During maximum heating the vitrinite particles undergo thermal heating which alters the nature of these particles within the rock. These maximum temperatures are ‘locked in’ by the vitrinite grains even after an exhumation period (Fig 5a). Thus, the measured vitrinite reflectance is an indicator of maximum temperature experienced by the rock. VR is a common analysis so is therefore widely available and is a decent maturity indicator. The maximum temperature measurements extracted from VR data may be converted to equivalent depth using appropriate techniques and compared to present-day depth of the sample to estimate the amount of exhumation (Corcoran and Clayton, 1999). Alternatively, a graph of depth versus VR plotted on a log scale (Dow, 1977) or depth versus temperature (Bray et al., 1992) may be used to estimate the amount of exhumation.

In this study, we employ the graphical approach initially proposed by Bray et al. (1992) to estimate the magnitude of exhumation in the basin. As a method, it is generally accepted as one of the most accurate methods for estimating exhumation using paleo thermal indicators and resolves some of the pitfalls of semi-log plots and empirical depth conversions (Corcoran and Doré, 2005). The technique has been used to quantify exhumation in several basins

including the Brooks Range, Alaska (O'Sullivan et al., 1995), Northern Australia basins (Duddy et al., 2003), Sichuan Basin, China (Zhu et al., 2019) and Bonaparte Basin, North West Shelf, Australia (Makuluni et al., 2021). The general procedure involved in using this method to estimate the magnitude of exhumation has been described below. In our study, only VR data was used to estimate the magnitude of exhumation, while VR data was integrated with AFTA from other independent studies to constrain the thermal history of the basin.

The method involves an initial conversion of VR values to equivalent temperature estimates. The Sweeney and Burnham (1990) kinetic model represents one of the most accurate and widely accepted VR to temperature translation models (Corcoran and Doré, 2005). We used this model to convert VR values to equivalent maximum temperatures, T (in °C) using an associated equation obtained from Yamamoto et al. (2005):

$$T = 158 + (90[\ln(Vr)]), \qquad (2)$$

where Vr indicates the mean maximum VR. As a basis for comparison, an empirical model (Barker and Pawlewicz, 1994) was also used to convert Vr to equivalent temperature values:

$$T = \big(\ln(Vr)\big) + 1.68)/0.0124. \qquad (3)$$

The well data for Vr and estimated maximum paleo-temperatures from Eqn. 2 and Eqn. 3 are presented in Table 1. These maximum temperature values were plotted against equivalent depth for individual wells. From these plots, maximum or paleo- temperature profiles for individual wells were established by fitting a linear relationship (line of best fit) between maximum paleo-temperatures and depth (example shown in Fig 5). Paleo-geothermal gradients were estimated from the paleo-temperature profiles at each well location (Fig. 5). Moreover, present-day temperature values obtained from drill-stem tests (DST) and corrected bottom-hole temperature (BHT) were plotted against depth to establish present-day temperature profiles and gradients for the individual wells (example shown in Fig 5). By extrapolating the maximum temperature profile to the paleo-surface (unconformity) and comparing it with the present-day temperature profile, the amount of exhumation at the unconformity can be estimated at each well location (Fig. 5; Bray et al., 1992). The estimated amount of exhumation is obtained by dividing the amount of cooling (temperature difference between the paleo-temperature and present-day temperature intercepts at the unconformity) by the paleo-geothermal gradient (Fig. 5; Bray et al., 1992; Corcoran and Doré, 2005; Green et al., 2002).

The method has some limitations including the following: vitrinite macerals are typically obtained from lithologies with high organic matter with very limited use for other lithologies (Corcoran and Clayton, 2001). Thus, the number of VR measurements down-well may not be enough to develop a good profile for calibration or for modelling purposes. Additionally, the method assumes that the paleo-geothermal signatures from the thermal indicators from VR are due to conductive heat flow resulting from depth of burial (Bray et al., 1992). Thus, results may be misleading in areas where stratigraphic units were affected by external heat sources such as magmatic bodies, hot fluids or areas that have experienced large increase in basal heat

flow (Corcoran and Doré, 2005). However, comparison of the present-day and paleo-temperature profiles can be used to identify such effects (Bray et al., 1992; O'Sullivan et al., 1995). As an additional constraint to the VR method, we have also considered the compaction-based technique, discussed in the next section.

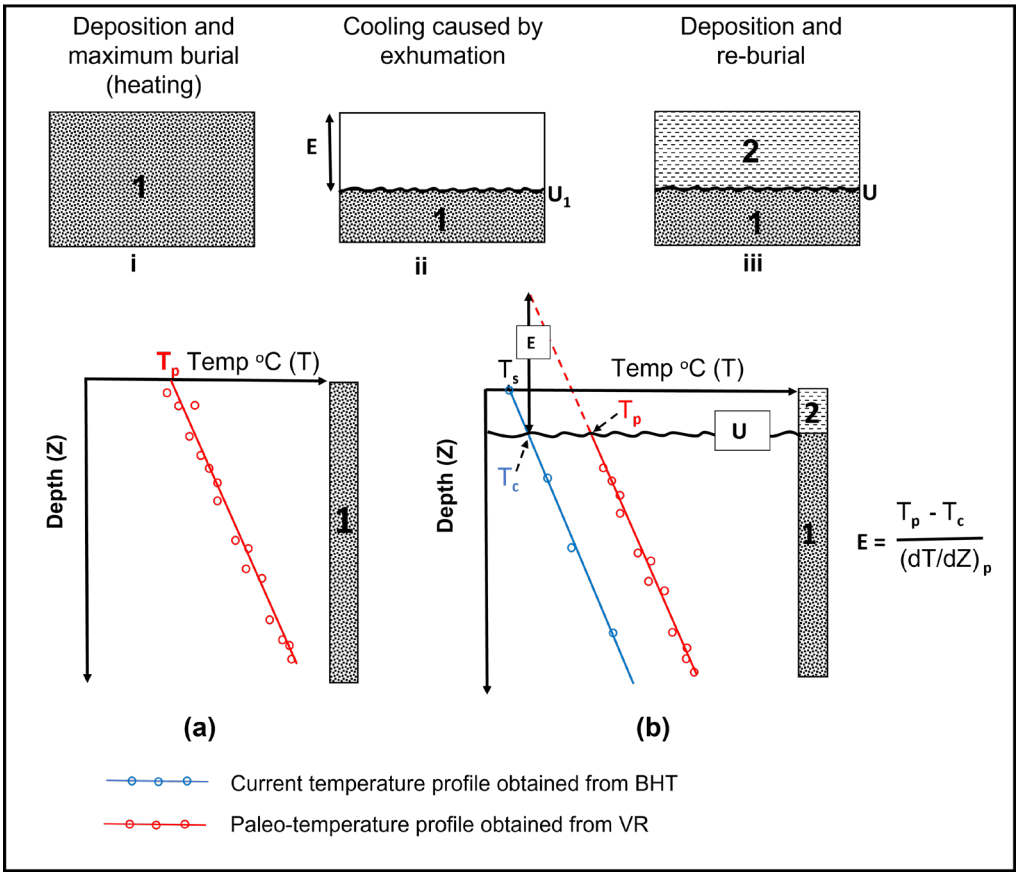

Figure 5. Schematic representation of estimating the amount of exhumation at an erosional unconformity using thermal-based technique [Modified from Corcoran and Doré (2005) and Bray et al. (1992)]. (a) Maximum temperatures are trapped in the vitrinite particles during maximum burial. (b) VR preserves these maximum temperatures even after a cooling event caused by exhumation. By comparing the paleo-temperature profile with the current (or present-day) temperature profile, the amount of exhumation can be estimated. E represents the amount of exhumation, T_p represents the temperature where the paleo-temperature profile intercepts the unconformity, T_c represents the temperature where the current temperature profile intercepts the unconformity and $(dT/dZ)_p$ represents the paleo-geothermal gradient estimated from the paleo-temperature profile.

3.2.3. Compaction-based technique for estimating the amount of exhumation.

The compaction-based method employs the porosity-depth reference to estimate the magnitude of exhumation at well locations. The advantages and limitations regarding the use of compaction-based techniques for estimating exhumation has been discussed in detail by Corcoran and Doré, (2005). This method uses sonic transit-time data (used as a proxy for porosity) that are widely available and are routinely acquired during well logging, which is one of its biggest advantages (Hillis, 1995; Tassone et al., 2014). Thus, the method provides greater spatial resolution compared to the limited data from paleo-thermal indicators, such as the VR

method above or apatite fission track data (Johnson et al., 2017). Furthermore, wireline logs including sonic logs are in situ measurements and are not affected by errors such as sample collection, preparation and processing (Tassone et al., 2014). Moreover, mechanical compaction is less susceptible to changes by transient heating, which is a major weakness associated with thermal-based techniques (Corcoran and Doré, 2005). However, the compaction-based technique cannot be used to independently constrain the timing of exhumation and this serve as the main limitation of the method (Tassone et al., 2014). Thus, in this study, we integrate the VR method above with a compaction-based method using stratigraphic data to constrain the timing of exhumation. A detailed description of the method is presented below.

The compaction technique is based on Athy's (1930) law which is govern by the fundamental principle that porosity reduces with increasing depth through burial and loading (mechanical compaction), and that this mechanism is largely irreversible (Licciardi et al., 2020; Magara, 1980). Diagenetic effects such as cementation and dissolution may also produce irreversible effects on the porosity of a sedimentary unit unrelated to burial (Allen and Allen, 2013). However, Tassone et al. (2014) argued that for normal basins that have not been affected by excessive convective or advective heating, these temperature-dependent diagenetic processes are mostly associated with depth of burial. These diagenetic processes are considered to be minimal for clastic sediments with burial depth ranging from 2 to 3 km (80 ^{0}C isotherm) (Corcoran and Doré, 2005). Also, Makuluni et al. (2021) argued that diagenetic effects including porosity enhancement through dissolution and porosity reduction through cementation generally counteracts and cancel out, leaving mechanical compaction as the main mechanism driving porosity reduction. Thus, the porosity of a sedimentary unit reflects the overall mechanical and thermochemical state of the unit and is a reflection of its maximum depth of burial (Tassone et al., 2014). Thus, the porosity of the sediments during maximum burial is retained during and even after exhumation (Licciardi et al., 2020). Although pore-elastic rebound (increase in porosity) resulting from unloading effects are recognised, these effects are considered to be negligible in comparison with loading effects (Tassone et al., 2014). As a result, most sedimentary units are compacted under equilibrium conditions (i.e. compaction under normal hydrostatic pressure) with no or negligible effects from overpressure or under-pressure (Allen and Allen, 2013; Magara, 1980). A basin's compaction pattern can therefore be represented by a single porosity-depth relationship (Licciardi et al., 2020). After an exhumation event in the geologic past, sedimentary units underlying the associated unconformity will show a present-day porosity, which is lower than expected for present-day burial depth (Hillis, 1995; Licciardi et al., 2020). By establishing a reference porosity-depth curve (which describes the normal compaction within the basin) and comparing that curve with the present-day porosity (obtained from core or well log), the difference in depth axis represents the potential exhumation that occurred between the time of maximum burial and the present-day at the well location (Corcoran and Doré, 2005; Hillis, 1995; Johnson et al., 2017; Licciardi et al., 2020). The approach has been used to quantify the amount of exhumation in several basins across the world including the Otway Basin, Australia (Tassone et al., 2014), Southern North Sea basins, UK (Corcoran and Doré, 2005; Hillis, 1995), Barents Sea, Norway (Licciardi et al., 2020), Broom Platform, Canning Basin, Australia (Johnson et al., 2017) and Bonaparte

Basin, North West Shelf, Australia (Makuluni et al., 2021). We focused our study on normally pressured clastic sedimentary units and looked out for signs of extreme cementation that may potentially serve as sources of errors. Interval sonic transit time data and core porosity are used to infer compaction (see section 3.1 for discussion) and have been used to estimate the amount of exhumation. The procedure is described below.

Gamma ray and density logs were combined with litho-stratigraphic descriptions from well completion reports to delineate interesting and laterally consistent sandstone and shale units. The gamma ray cut off for shale intervals was 130 API, and the upper limit for sandstone intervals was 30 API. In the case of sandstones, corrected sonic interval transit time data within selected sandstone units were converted to porosity using the well-known Wyllie et al. (1956) time average equation (Eqn. 4). This is one of the commonly used technique in the Petroleum Industry for converting interval transit time to porosity in sandstone lithologies (Crain, 2002).

$$\Phi = \frac{\Delta t_{log} - \Delta t_{ma}}{\Delta t_f - \Delta t_{ma}} \quad , (4)$$

where, Φ = porosity, Δt_{log} = logged compressional sonic interval transit time, Δt_{ma} = standard sonic transit time for matrix material (55 us/ft for sandstone), Δt_f = standard sonic transit time for pore fluid. Well completion report indicate formation water in the selected sandstone units. Thus, a standard value of 189 us/ft was used. These standard parameters were obtained from Crain (2002).

Filtered interval transit time (compressional sonic velocity data) from the selected sandstone and shale units and their equivalent depths were plotted and compared with the reference porosity-depth curve. In the case of the sandstone, both the measured core porosity and log porosity data from the units were plotted on the reference curve. The reference curve is a standard porosity versus depth curve or transit time versus depth curve that describes porosity reduction with depth (Athy, 1930) representing sedimentary units at their maximum burial depth (Hillis, 1995; Tassone et al., 2014). The vertical displacement of the data from this reference curve is the estimated amount of exhumation (Licciardi et al., 2020). Reference curves are normally obtained from well locations in the basin where sedimentary units are presently at their maximum burial depth (Dentith, 2012; Hillis, 1995). That is, areas within the basin that have not experienced exhumation. However, considering that the entire Kidson Sub-basin has experienced multiple significant exhumation periods (Shaw et al., 1994), obtaining a reference curve for the basin will lead to inaccurate results by significantly underestimating the amount of exhumation (Hillis, 1995). Thus, reference curves for the shale (transit time data) and sandstone (porosity data) were obtained using other alternative published methods. For the shale compaction technique, we followed the approach employed by Johnson et al. (2017). The reference curve was obtained from a standard shale compaction curve that describes normal velocity-depth relationship for shales (Fig. 6a). For the sandstone compaction technique, we followed the approach presented in Corcoran and Doré (2005) and (Makuluni et al., 2021).

Thus, the reference curve was constructed following Athy's (1930) porosity-depth trend (Eq. 5; Fig 6b). Standard lithological parameters for sandstone were obtained from Allen and Allen (2013) and Sclater and Christie (1980). The equation defining the reference curve is given as

$$\Phi = \Phi_0 e^{-cy} , \qquad (5)$$

where, Φ = measured porosity, Φ_0 = surface porosity (0.56 for sandstone), c = compaction coefficient (0.39 km^{-1} for sandstone) and y = depth.

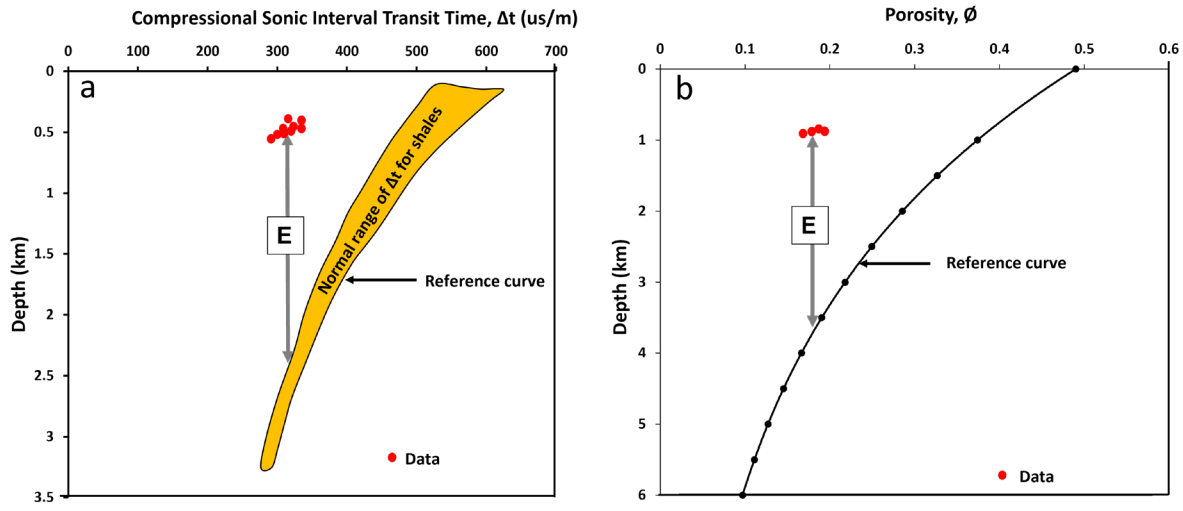

Figure 6. Approach to estimate the magnitude of exhumation (E) using compaction-based method Depth difference between the plotted porosity or interval transit time data and the reference curve represents the amount of exhumation. (a) Reference curve represents standard compaction curve for shales from interval transit time data [After Johnson et al. (2017)]. (b) Standard reference curve for sandstone lithology [After *(Athy, 1930; Corcoran and Doré, 2005; Makuluni et al., 2021)].*

After obtaining the reference curve, porosity or sonic interval transit time from stratigraphic units immediately below the specified unconformity that meet the necessary requirements (stratigraphically equivalent, thick and laterally extensive) were used to constrain the amount of exhumation. These requirements are to ensure that similar lithotypes are used across the individual well locations and to avoid facies related transit-time or porosity variations (Dentith, 2012; Hillis, 1995).

Multiple periods of exhumation may be derived from the same well for scenarios similar to the Kidson Sub-basin where lower stratigraphic units were at maximum burial before upper stratigraphic units due to an intervening erosional episode. Different burial anomaly curves may be constructed for the different stratigraphic units, but the lower unit should have a deeper burial anomaly than the upper unit (Japsen, 2000). The deviation between the compaction data for a unit and it's burial anomaly (reference curve), provides an estimate of how much deeper

that unit has been buried which is equivalent to the amount of exhumation at one specific time after deposition (Japsen, 2000). Alternatively, compaction data from the different stratigraphic units in the well may be compared with the a standard reference curve to estimate exhumation at different periods (Corcoran and Doré, 2005; Johnson et al., 2017; Makuluni et al., 2021). In that case, assuming successive burials do not exceed the previous maximum burial depth, the lower unit will experience the higher amount of exhumation after maximum burial because it contains records of multiple exhumation and subsidence phases until the present-day. Thus, the magnitude of exhumation for the upper unit may be deducted from that of the lower unit to obtain exhumation for shorter or specific exhumation intervals (Makuluni et al., 2021). This approach was employed for this study. The selected sandstone and shale units were tied to chrono- and litho- stratigraphic data as well as the geological history of the basin to constrain the approximate timing of exhumation. The selected units provide information on the exhumation that occurred immediately after their deposition. Thus, the Poole, Tandalgoo and middle Carribuddy sandstones and shale units have been carefully selected to constrain the amount of exhumation during the Late Triassic-Early Jurassic, middle Carboniferous, and Late Silurian-Early Devonian exhumation episodes respectively (Fig. 3 and 6).

4. Results

4.1. Interpretation of Seismic line 18GA-KB1-60km.

Seismic line 18GA-KB1-60km covers the tectonic units of the Canning Basin and include the Pilbara Craton, Wallal Embayment, Barnicarndy Graben, Ankatell Shelf, Kidson Sub-basin and Ryan shelf (Fig. 7). For the purposes of this study, interpretation has been focused on the Kidson Sub-Basin. According to the seismic line, the Kidson Sub-basin is about 400 km wide and 6.3 km deep at the location of the seismic line, and contains well preserved sediments seen as reflectors in the seismic section (Fig. 7). Sediments were deposited in a depocenter created between two basement highs (Ankatell and Ryan shelves) during the early extensional phase of the basin in the Early Ordovician (Fig. 7). These basement highs are shown by the chaotic seismic reflections pattern at the edges of the Kidson Sub-basin. The reflectors are continuous and traceable across the entire basin, implying that major geological events, including deposition and erosion, occurred there continuously (Fig. 7). In general, most reflectors show conformable relationships across the basin indicating continuous deposition episodes (Fig. 7). Few reflectors show unconformable relationships, which extend across the entire basin indicating a break in deposition (unconformity) and are discussed in the following section. Extensional structures shown as normal faults are observed within the deeper parts of the Sub-basin which demonstrate early rifting episodes that developed and shaped the basin during the early Paleozoic period (Fig. 7; Southby et al., 2019). Compressional and inverted structures, including faulting and upright folds, are observed within the entire stratigraphic package, from Silurian to Mesozoic sediments, at the eastern and western edges of the Kidson Sub-basin (Fig. 7a). We interpret these to be the result of major compressional and transpressional episodes that affected the basin during the Paleozoic and Mesozoic periods and resulted in extensive uplift, erosion, tilting and folding of sedimentary units (Hashimoto et al., 2018; Shaw et al., 1994). Litho-stratigraphic control from wells in the basin indicate that the Ordovician to Devonian sequence is dominated by mixed clastics, carbonates and evaporite sequences

(example, Goldwyer Formation, Carribuddy Group) unconformably overlain by clastic dominated carboniferous to Mesozoic sequences (example Grant Group, Poole Sandstone) (Fig. 7b).

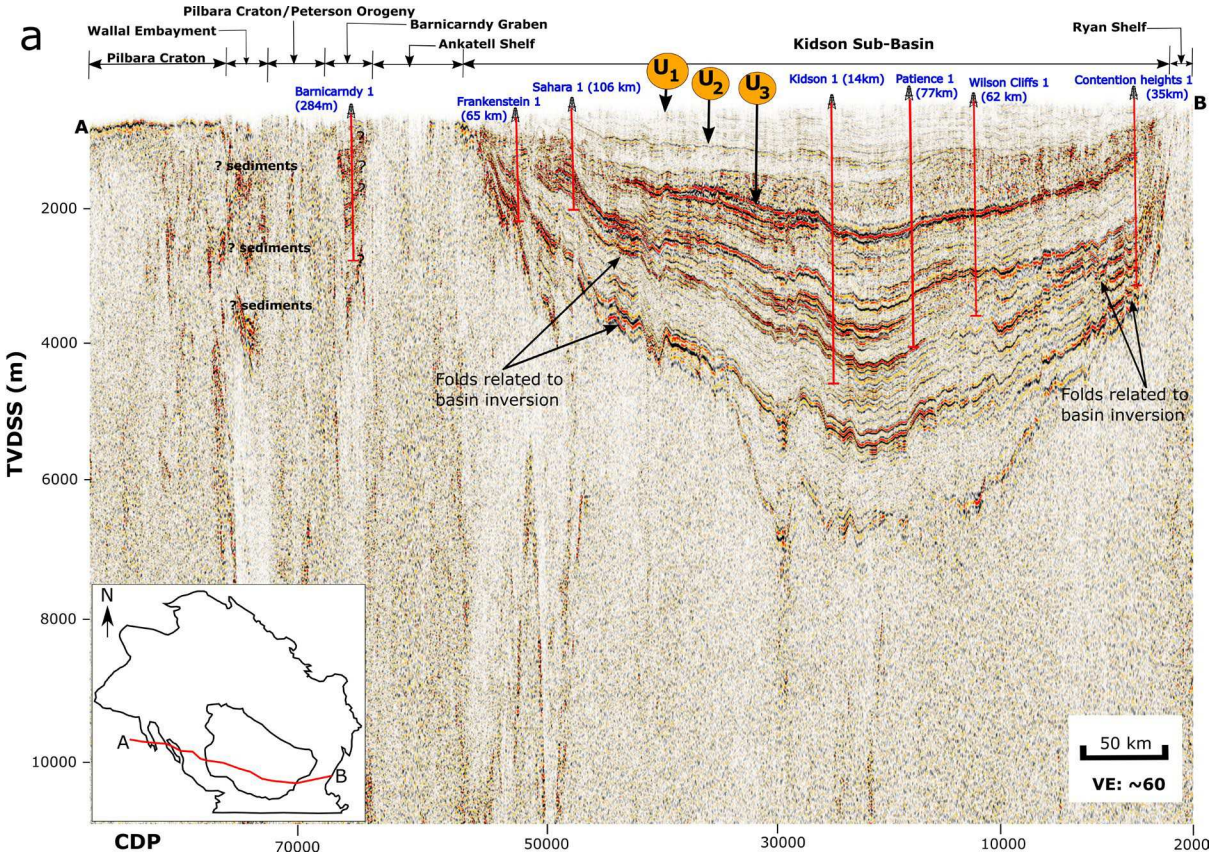

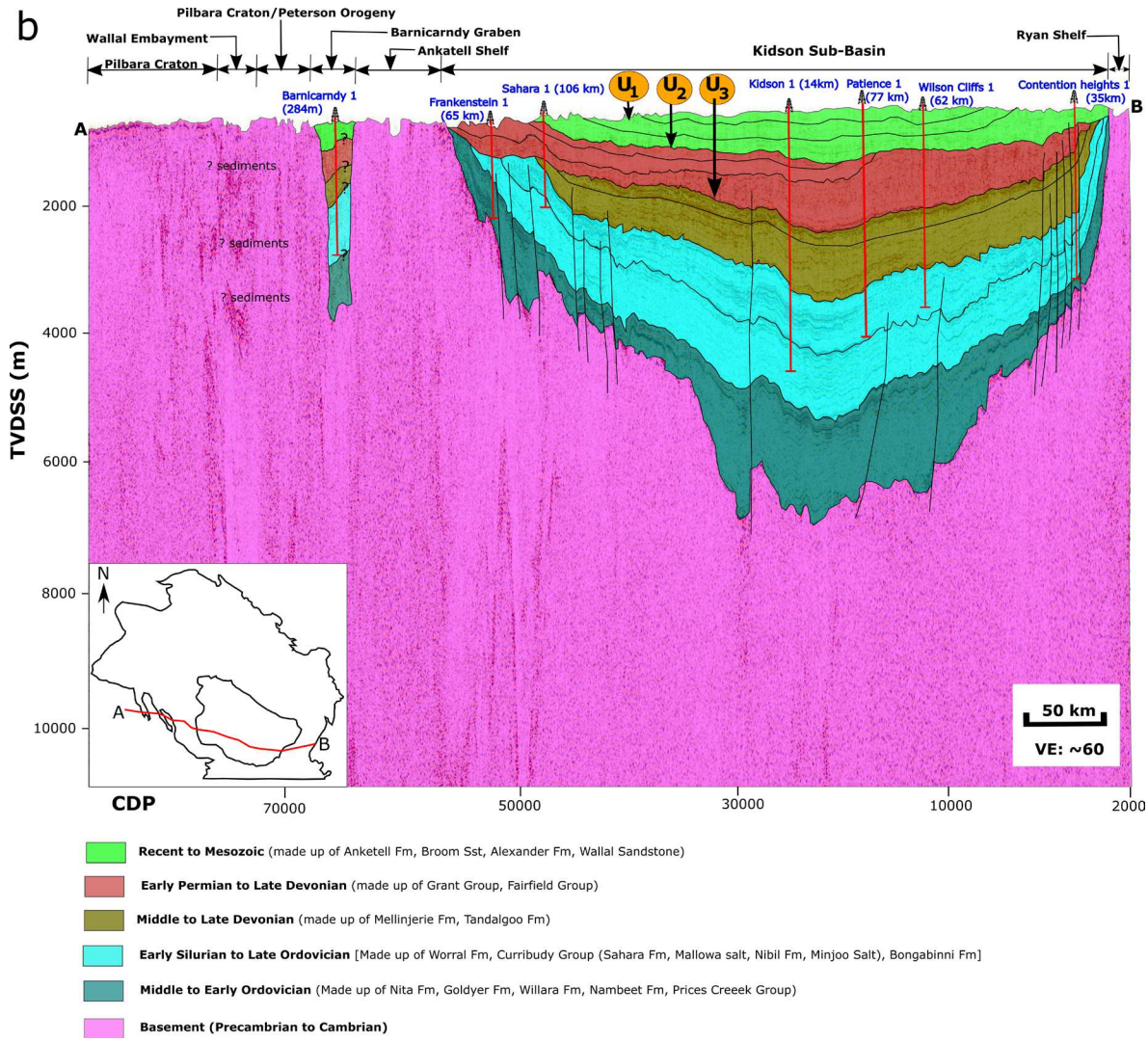

Figure 7. a.) Un-interpreted and b.) interpreted seismic profile (section) of line 18GA-KB1-60km TVDSS is true vertical depth Subsea, CDP is common depth point and VE is vertical exageration. Inset (bottom left corner) is the map of the Canning Basin showing the location of the Kidson Sub-basin and seismic line. Interpretation shows the basin structure and major faults within the Kidson Sub-basin, as well as the location and extent of erosional unconformities associated with exhumation. These angular unconformities, labelled U_1, U_2 and U_3 correspond to Cenozoic, Early Jurassic, and middle Carboniferous exhumation periods.

4.2. Unconformities in the Kidson Sub-basin

Seismic data and stratigraphic information from well data, such as well completion reports have been integrated with the overall evolution of the basin to give a detailed analysis of the unconformities in the Kidson Sub-basin. A detailed stratigraphic chart, showing the relationship between lithostratigraphic units and major unconformities is shown in Fig. 3. In general, we identified four major unconformities and are labelled from U_1 to U_4 (Fig. 3). We identified and interpreted unconformities U_1, U_2 and U_3 on seismic line 18GA-KB1-60km. They are observed to extend across the entire Kidson Sub-basin (Fig. 7). On seismic profiles, these obvious strata-discordant relation at these boundaries indicate an angular unconformity where older units are truncated by erosion and then superimposed by younger units (Fig. 7). In

relation to the geological history of the basin, we interpret these angular unconformities as erosional surfaces following major periods of inversion that resulted in extensive uplift and erosion across the basin (Figs. 3 and 7). We interprete unconformity U_1, as a period of non-deposition or minor erosion associated with the collision of Australian and Indian Sub-plates during the Tertiary era (Eocene ca. 40-45 Ma) (Fig. 3 and 5; Keep et al., 2007). Although a break-up unconformity has been suggested during the middle Cretaceous period (Fig 3; Hashimoto et al., 2018), it appears to have no strong correlation with major exhumation in the Canning Basin. We associate unconformity U_2 with the Fitzroy Transpressional movement, which resulted in extensive exhumation in the Canning Basin during the Late Triassic to Middle Jurassic periodd (230 to 180 Ma) (Fig. 3 and 7). We associate unconformity U_3, with transpressional tectonics, the Meda Transpressional Movement, which resulted in extensive exhumation in the basin during the middle to late Carboniferous time (from 330 to 200 Ma) (Fig. 3 and 7). The unconformity U_4 has not been observed on seismic profiles, but note that it has been reported in well completion reports and documented as part of the evolution of the basin (Fig 3; Hashimoto et al., 2018). We associated unconformity U_4 with the compressional deformation, the Prices Creek Compressional Movement, that led to exhumation during the Middle Silurian to Early Devonian (from 420 to 400 Ma) (Fig. 3 ; Parra-Garcia et al., 2014; Shaw et al., 1994). We were not able to constrain the magnitude of exhumation at unconformity U_1 because well stratigraphic data indicated that the post Jurassic sediments have been removed at the various well locations leaving the Early Jurassic unconformity, U_2 at or close to the surface. Moreover, the Cenozoic inversion that resulted in U_1 is suggested not to have had significant effects on the onshore Canning Basin (Shaw et al., 1994). Since unconformities U_2, U_3 and U_4 are the results of major exhumation events in the basin, they are the focus of this study. Thus, the amount of exhumation at these unconformities have been estimated and results are presented in the next section.

4.3 Magnitude and uncertainties in exhumation estimates from VR data

Results from AFTA from several wells across the Canning Basin indicate that cooling from maximum post-depositional temperatures occurred in the Late Triassic to Early Jurassic (see section 5.1; Duddy et al., 2006, 2003; Green, 2014) associated with the Fitzroy Transpression. This imply that a paleothermal maximum was attained during the Early Triassic extension, prior to the Fitzroy Transpression. Since VR is a maximum temperature indicator, temperature information obtained from VR during paleothermal maximum is only appropriate to constrain the succeeding exhumation event (Corcoran and Doré, 2005). Thus, the magnitude of exhumation during the Late Triassic to Early Jurassic inversion episode (Fitzroy Transpression, U_2) has been estimated using VR and results are summarised in Table 3 and displayed in Fig. 8. Results indicate that the magnitude of exhumation ranged from 800 to 2400 m and increased from south east to northwest across the Kidson Sub-basin (Fig. 12A2). Uncertainty analysis associated with the estimated magnitude of exhumation is discussed in the next section.

General uncertainties regarding the use of VR for exhumation estimates have been described in detail by Corcoran and Doré (2005). For this study, caved-in, suppressed and reworked VR, as well as VR data affected by external localised heat bodies, where identified were not used

for analysis. However, there may be uncertainties associated with the quality of VR data associated with the number of sample runs (N) used to obtain each VR data point. Although, 'N' at most well locations is not known, 'N' obtained for Kidson-1 and Contention Heights-1 is small for some samples and may have uncertainty on the quality of VR data and associated exhumation estimate. In this study, we associate uncertainties in exhumation estimates to the limited VR data points in the selected wells used to constrain paleo-geothermal profiles at the individual well locations. This effect is most pronounced in Nicolay-1, Sahara-1 and Contention Heights-1 wells, which have the least VR data points. We have employed a range of possible paleo-geothermal gradients to analyse the resulting uncertainties in the exhumation estimates derived from these wells. In general, a 5^0C/km decrease in the estimated paleo-geothermal gradient, will result in about 300 to 500 m increase in the estimated magnitude of exhumation and a 5^0C/km increase in the estimated paleo-geothermal gradient, will result in about 300 to 400 m reduction in the estimated amount of exhumation. The detailed uncertainty results are presented in Table 3.

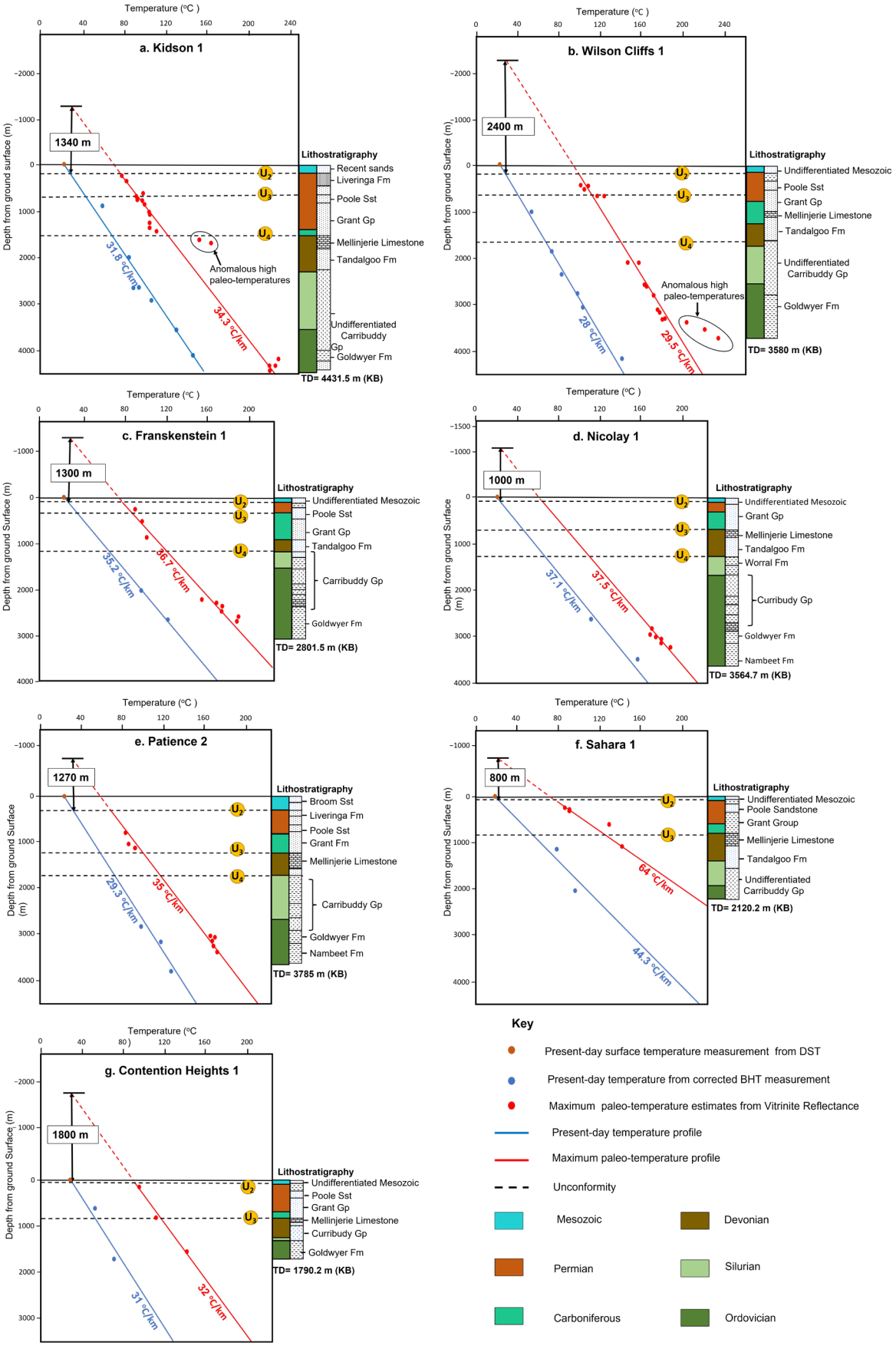
a. Kidson 1
Temperature (°C)
Depth from ground surface (m)
1340 m
31.8 °C/km
34.3 °C/km
Anomalous high paleo-temperatures
Lithostratigraphy
Recent sands
Liveringa Fm
Poole Sst
Grant Gp
Mellinjerie Limestone
Tandalgoo Fm
Undifferentiated Carribuddy Gp
Goldwyer Fm
TD= 4431.5 m (KB)
b. Wilson Cliffs 1
2400 m
28 °C/km
29.5 °C/km
Anomalous high paleo-temperatures
Undifferentiated Mesozoic
Poole Sst
Grant Gp
Mellinjerie Limestone
Tandalgoo Fm
Undifferentiated Carribuddy Gp
Goldwyer Fm
TD= 3580 m (KB)
c. Franskenstein 1
1300 m
35.2 °C/km
36.7 °C/km
Undifferentiated Mesozoic
Poole Sst
Grant Gp
Tandalgoo Fm
Carribuddy Gp
Goldwyer Fm
TD= 2801.5 m (KB)
d. Nicolay 1
1000 m
37.1 °C/km
37.5 °C/km
Undifferentiated Mesozoic
Grant Gp
Mellinjerie Limestone
Tandalgoo Fm
Worral Fm
Curribudy Gp
Goldwyer Fm
Nambeet Fm
TD= 3564.7 m (KB)
e. Patience 2
1270 m
29.3 °C/km
35 °C/km
Broom Sst
Liveringa Fm
Poole Sst
Grant Fm
Mellinjerie Limestone
Carribuddy Gp
Goldwyer Fm
Nambeet Fm
TD= 3785 m (KB)
f. Sahara 1
800 m
64 °C/km
44.3 °C/km
Undifferentiated Mesozoic
Poole Sandstone
Grant Group
Mellinjerie Limestone
Tandalgoo Fm
Undifferentiated Carribuddy Gp
TD= 2120.2 m (KB)
g. Contention Heights 1
1800 m
31 °C/km
32 °C/km
Undifferentiated Mesozoic
Poole Sst
Grant Gp
Mellinjerie Limestone
Curribudy Gp
Goldwyer Fm
TD= 1790.2 m (KB)
Key
Present-day surface temperature measurement from DST
Present-day temperature from corrected BHT measurement
Maximum paleo-temperature estimates from Vitrinite Reflectance
Present-day temperature profile
Maximum paleo-temperature profile
Unconformity
Mesozoic
Devonian
Permian
Silurian
Carboniferous
Ordovician

Figure 8. Magnitude of estimated exhumation using VR data for wells in the Kidson Sub-basin during the Late Triassic to Early Jurassic exhumation event (Fitzroy Transpression). Estimates have been made at unconformity U_2 (see section 4.3 for discussion). Numbers written in blue represent present-day geothermal gradient and numbers written in red represent paleo-geothermal gradient.

Table 3. Magnitude and uncertainties in exhumation estimates from VR data.

Well name	5 ^{0}C/km lower	**Actual (Likely) ***	5 ^{0}C/km higher
Kidson-1	1570	**1340**	1170
Willson Cliffs-1	2940	**2400**	2060
Frankenstein-1	1514	**1300**	1150
Nicolay-1	985	**1000**	753
Patience-2	1333	**1270**	1000
Sahara-1	763	**800**	652
Contention Heights-1	2200	**1800**	1649

***Maximum likelihood estimates of the amount of exhumation

4.4 Magnitude of exhumation from compaction method

The magnitude of exhumation using shale and sandstone compaction techniques are presented in Fig. 9 and 10, as well as in Table 4 and 5. Results from both methods are consistent and indicate that the Kidson Sub-basin has experienced a total amount of exhumation up to 2400 m from Late Silurian-Early Devonian to present-day, 1850 m from the middle Carboniferous to present-day, and 1200 m from Late Triassic-Early Jurassic to present-day (Fig. 9, 10, 11; Table 4). Also, results indicate that about 350 to 500 m of exhumation occurred during the middle Silurian to Early Devonian inversion episode (Table 5; Fig. 12C). We associate this exhumation to the Prices Creek Compression which resulted in unconformity U_4 (Fig. 3). During this episode, the magnitude of exhumation increased from southeast to northwest across the Kidson Sub-basin (Fig. 12C). Additionally, results indicate that 500 to 750 m of exhumation occurred during the middle Carboniferous (Table 5; Fig. 12B). We associate this exhumation to the Meda Transpression which resulted in unconformity U_3 (Fig 3 and 7). During this event, the magnitude of exhumation increased from south to north across the sub-basin (Fig. 12B). Furthermore, 800 to 1200 m of exhumation occurred during the Late Triassic to Early Jurassic period (Table 5; Fig 12A1) and we associate this exhumation to the Fitzroy Transpression which produced unconformity U_2 (Fig. 3 and 7). During this period, the magnitude of exhumation increased from southeast to northwest across the sub-basin. In general, results for the three exhumation periods employed for this study indicate that the magnitude of exhumation during later inversion episodes were higher than earlier inversion episodes with highest estimates recorded during the Late Triassic to Early Jurassic exhumation (Fig. 12).

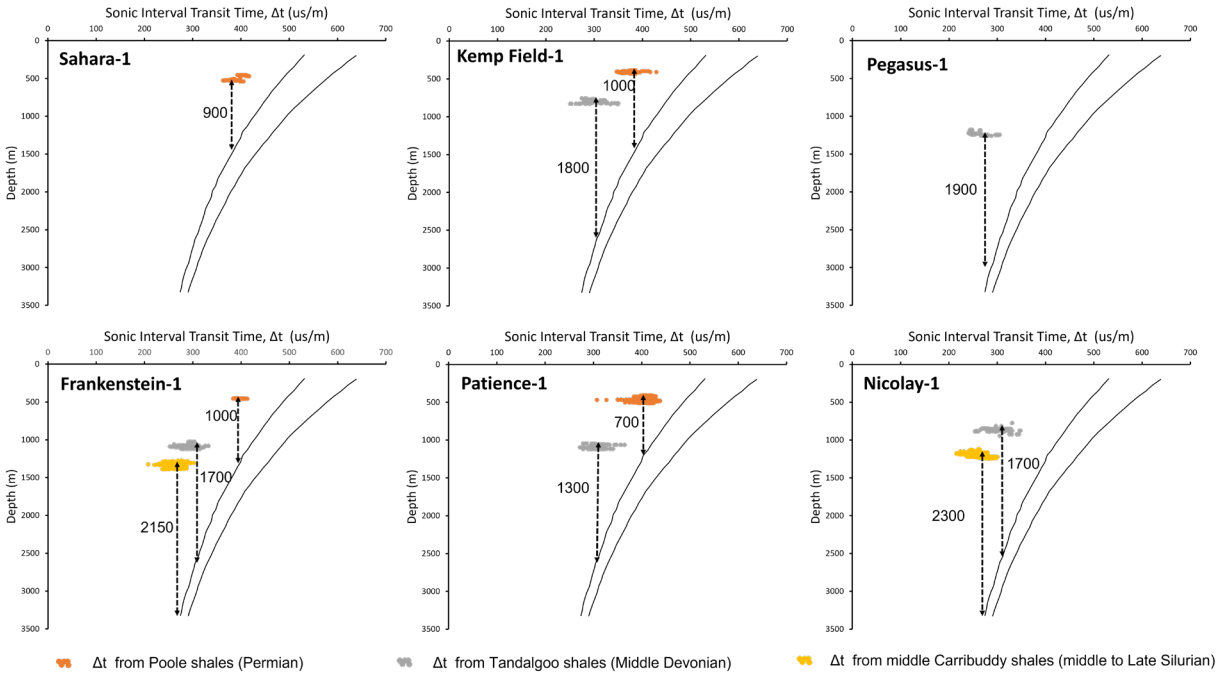

Figure 9. Magnitude of exhumation estimates from shale compaction. Sonic transit time measurements from Poole, Tandalgoo and Carribuddy shale lithologies have been plotted and compared with the reference curve to constrain the magnitude of exhumation since the Late Triassic-Early Jurassic, middle Carboniferous and Late Silurian-Early Devonian periods, respectively.

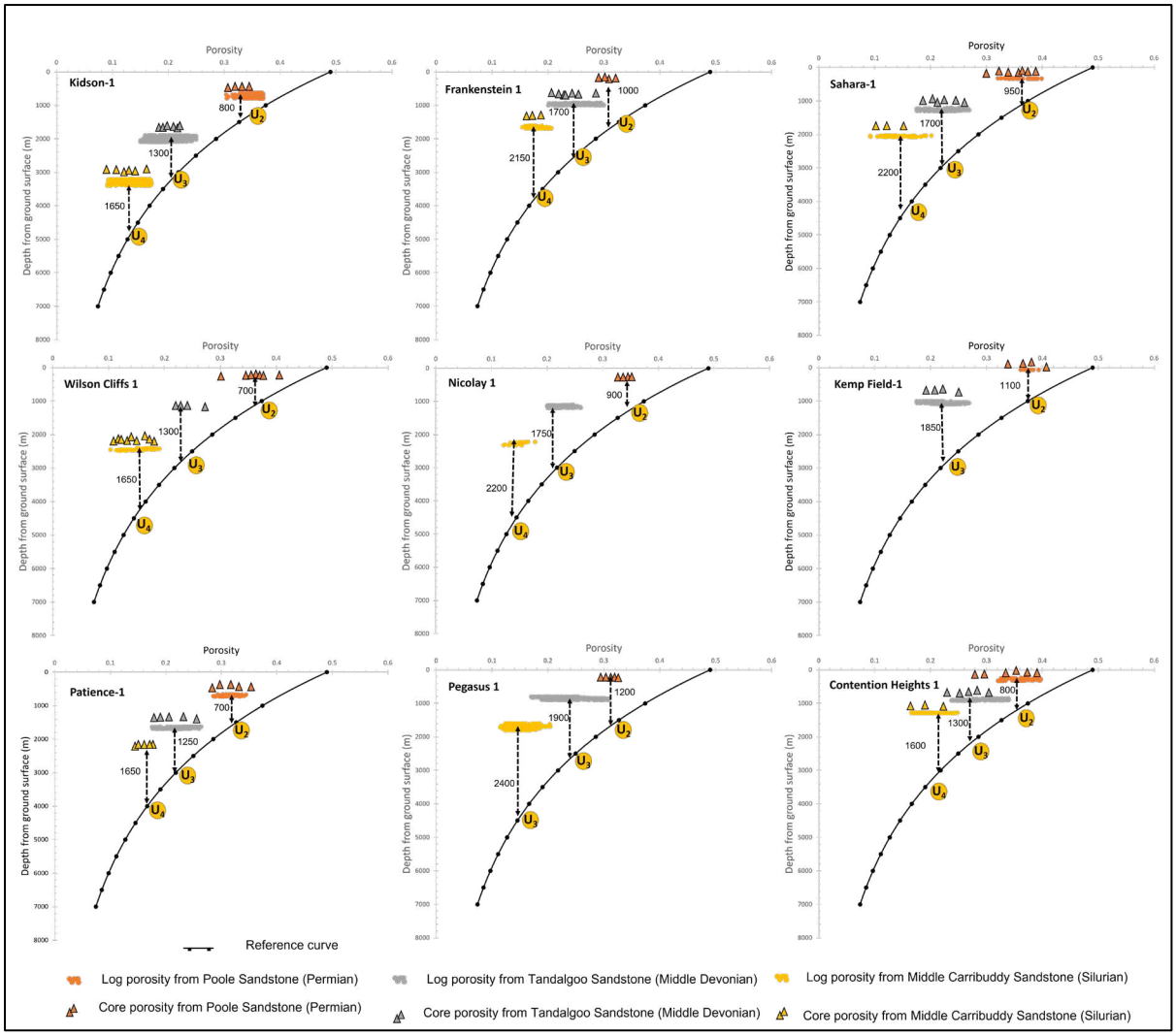

Figure 10. Magnitude of exhumation estimates from sandstone compaction. Core and log porosity measurements from the *Poole, Tandalgoo and Carribuddy sandstones have been plotted and compared with the reference curve to constrain the magnitude of exhumation since the Late Triassic-Early Jurassic (U_2), middle Carboniferous (U_3) and Late Silurian-Early Devonian (U_4) time periods, respectively.*

Table 4. Total amount of exhumation since the Late Triassic-Early Jurassic, middle Carboniferous and Late Silurian-Early Devonian using compaction method.

Well Name	Sandstone Compaction			Shale Compaction		
	Early Jur	Mid Car	Early Dev	Early Jur	Mid Car	Early Dev
Kidson-1	800	1300	1650	-	-	-
Frankenstein-1	1000	1700	2150	1000	1700	2150
Sahara-1	950	1700	2200	900	-	-
Wilson Cliffs-1	700	1300	1650	-	-	-
Nicolay-1	900	1750	2200	-	1700	2300

Pegasus-1	1200	1900	2400	-	1900	-
Kemp Field-1	1100	1850	-	1000	1800	-
Patience-1	700	1250	1650	700	1300	-
Auld-1	1000	1650	-	-	-	-
Auld South-1	950	1600	-	-	-	-
Contention Heights-1	800	1300	1600	-	-	-
Gibb Maitland-1	900	1650	2000	-	-	-

Dash (-) represents no data

Table 5. Amount of exhumation during Late Triassic-Early Jurassic, middle Carboniferous and Late Silurian-Early Devonian inversion episodes.

Well Name	**Early Jurassic**			Compaction	
	Thermal (VR)[1]	Comp	Absolute Difference	Mid Car	Early Dev
Kidson-1	1340	800	540	500	350
Frankenstein-1	1300	1000	300	700	450
Sahara-1	800	950	150	750	500
Wilson Cliffs-1	2400	700	1700	600	400
Nicolay-1	1000	900	100	750	490
Pegasus-1	-	1200	-	700	550
Kemp Field-1	-	1100	-	750	-
Patience-2	1270	700	570	570	350
Auld-1	-	1000	-	650	-
Auld South-1	-	950	-	600	-
Contention Heights-1	1800	800	1000	500	300
Gibb Maitland	-	900	-	750	350

Dash (-) represents no data

[1]Maximum likelihood estimates

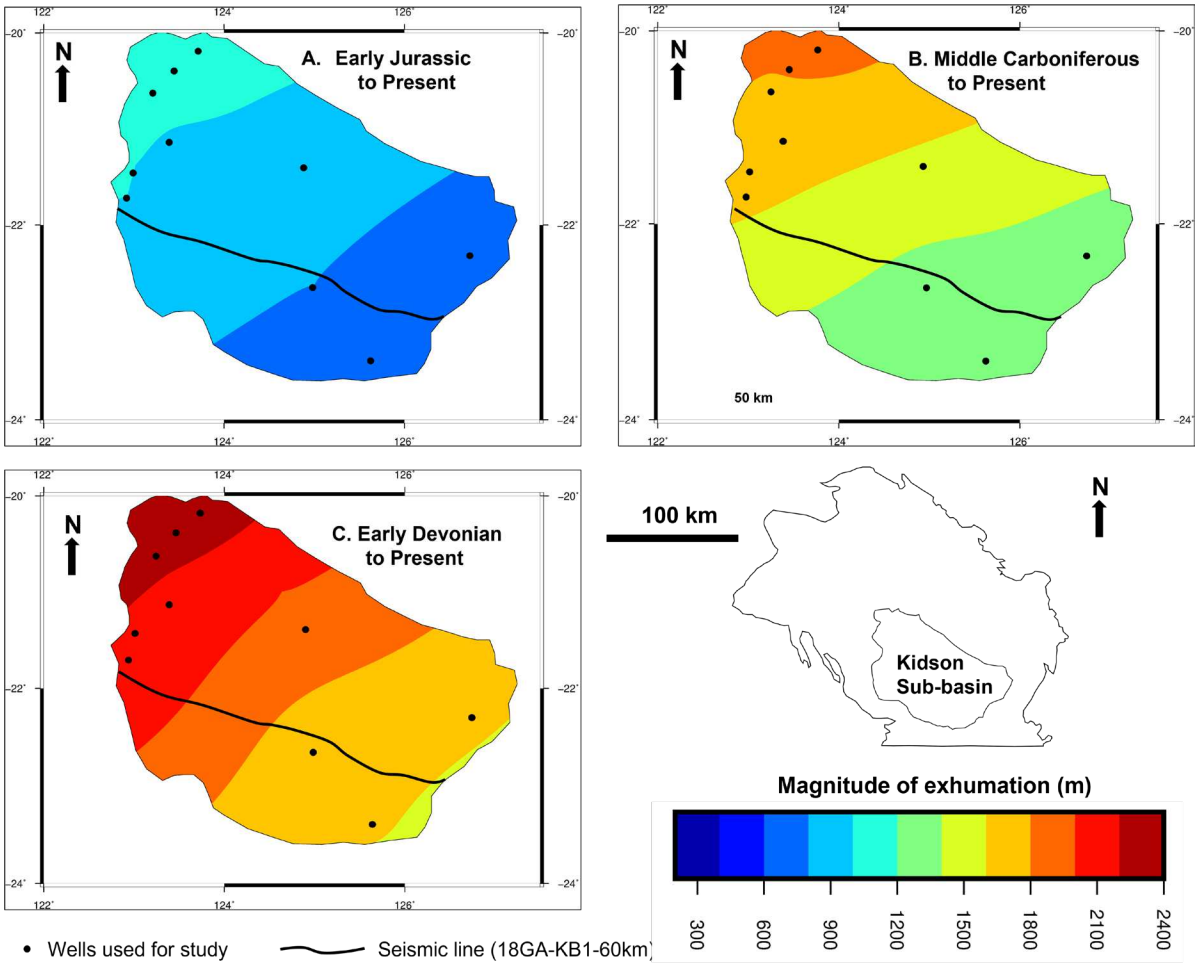

Figure 11. Map showing the distribution of the total amount of exhumation the Kidson Sub-basin using compaction technique. The location of seismic line 18GA-KB1-60km (black line) and distribution of wells (black dots) used in this study are also shown. Bottom right corner is a base map showing the Kidson Sub-basin within the Canning Basin. A) magnitude of exhumation from the Late Triassic-Early Jurassic to present. B) magnitude of exhumation from the middle Carboniferous to present. C) magnitude of exhumation from the Late Silurian-Early Devonian to present. Maps have been interpolated using the results from the wells. Interpolation was done using GMT surface (Wessel et al., 2019) with grid table data that uses adjustable tension continuous curvature splines.

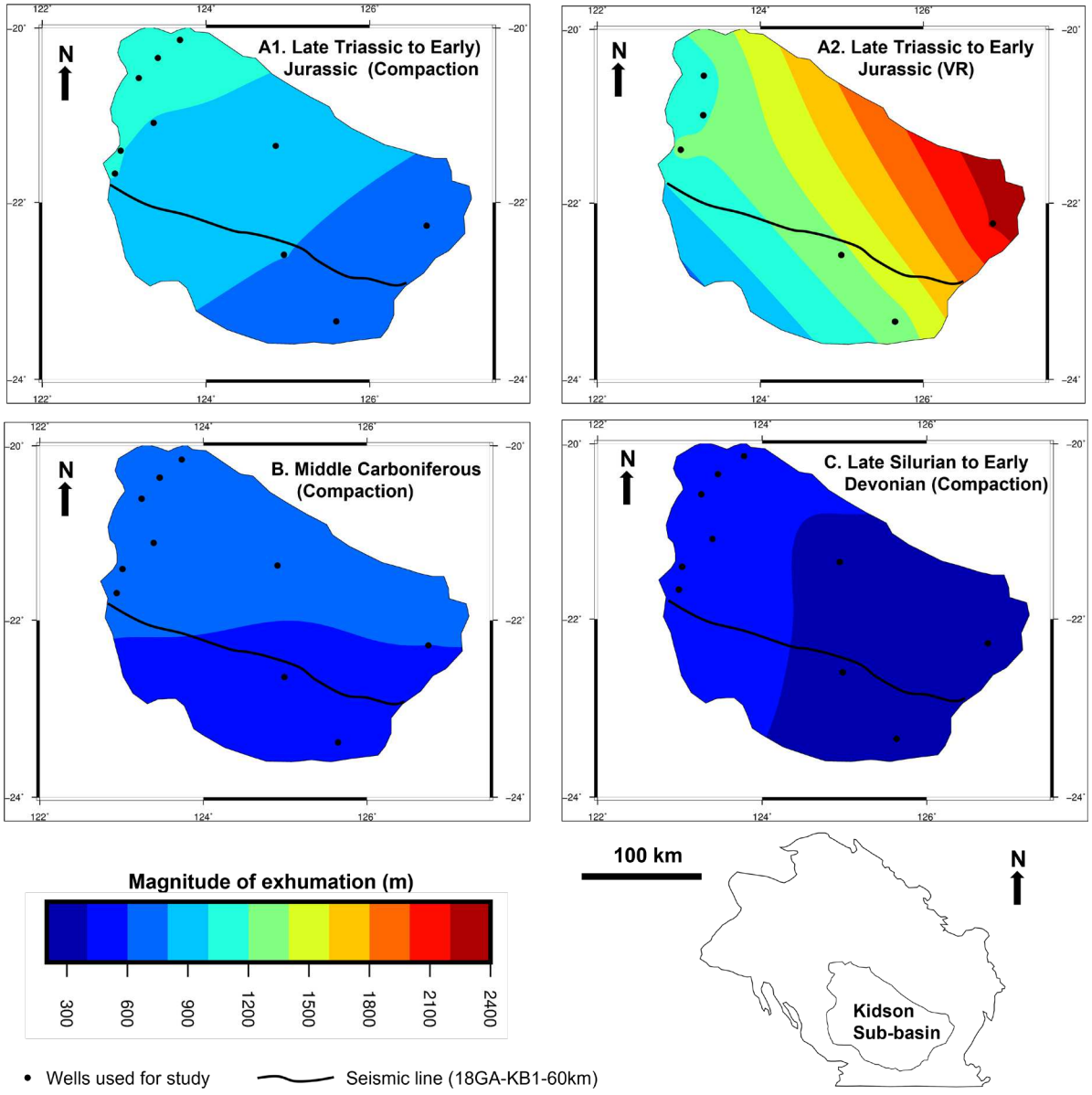

Figure 12. Map showing the distribution of the amount of exhumation in the Kidson Sub-basin. The location of seismic line 18GA-KB1-60km (black line) and distribution of wells (black dots) used in this study are also shown. Bottom right corner is a base map showing the Kidson Sub-basin within the Canning Basin. A1) Magnitude of exhumation during the Late Triassic to Early Jurassic exhumation episode (associated with Fitzroy Transpression) using the Compaction (porosity) method. A2) Magnitude of exhumation during the Late Triassic to Early Jurassic (associated with Fitzroy Transpression) using the thermal (VR) method. B) Magnitude of exhumation during the middle Carboniferous (associated with Meda Transpression). C) Magnitude of exhumation during the Late Silurian to Early Devonian (associated with the Prices Creek compression). Maps have been interpolated using the results from the wells.

5. Discussion

5.1 Exhumation Estimates from Thermal and Compaction Methods.

The estimated magnitude of exhumation during the Late Triassic to Early Jurassic from both the thermal and compaction method have been compared (Table 5). The two techniques gave contrasting results. Results from the compaction method indicate that the amount of exhumation increased from east to west across the Kidson Sub-basin (Fig. 12A1). On the other hand, results from the thermal technique indicate that the magnitude of exhumation generally increased from west to east across the Kidson Sub-basin (Fig. 12A2). Also, results indicate that the thermal method yielded higher exhumation estimates at all the well locations, except for Sahara-1. Large uncertainties associated with temperature profiles and gradients associated with Sahara-1 have been discussed above. At all the other well locations, where the thermal method yielded higher exhumation estimates, differences in the estimated magnitude of exhumation between the two methods range from as low as 100 m to as high as 1700 m (Table 5). Reasons accounting for the contrasting pattern of exhumation distribution between the two methods and comparatively higher exhumation estimates associated with the thermal method are discussed below. Here, we disregard potential uncertainties and errors that may be associated with data acquisition and sampling as well as errors that may be associated with analytical, processing and systematic techniques since their impact on the data cannot be recognised. These uncertainties may include sonic and VR data quality and the VR to temperature translation model.

Observations from temperature-depth plots for Kidson-1 and Wilson Cliffs-1, located within the eastern part of the Kidson Sub-basin indicate anomalous high temperature measurements interpreted as reworked vitrinite or the effect of localised heating (Fig. 8a and 8b). Although the source of these anomalous high temperatures is inconclusive, they are only observed within the eastern part of the basin. Moreover, the difference in the magnitude of exhumation estimated using the thermal method are extremely high compared to estimates from the compaction method at these well locations with differences of 540 m and 1700 m at Kidson-1 and Wilson Cliffs-1 respectively (Table 5). Although, other wells including Patience-2 and Contention Heights-1 located within the eastern part of the basin do not show any anomalous high temperature data, they also show similar pattern where the thermal technique yielded very high exhumation estimates compared to the compaction technique (Table 5). Differences in the magnitude of exhumation are 570 m and 1000 m for Patience-2 and Contention Heigths-1 respectively.

However, wells located within the western part of the sub-basin, including Frankenstein-1 and Nicolay-1 do not show anomalous temperature data points. Also, at these well locations, there is very small variation in exhumation estimates between both methods with differences of 200 m and 100 m for Frankenstein-1 and Nicolay-1 respectively (Table 5). This small variation in exhumation estimates between the compaction and thermal method are consistent with other studies where both techniques have been employed and where no anomalous high temperature measurements were reported. For example, results from the UK Southern North Sea indicate that the thermal technique using VR and AFTA yielded higher estimates in the order of 300 to

500 m greater than estimates using the compaction method (sonic transit time) at the various well location (Hillis, 1995). Also, in the Southern Bonaparte Basin, the thermal technique yielded higher estimates ranging from 20 to 750 m higher than the compaction method (Makuluni et al., 2021). This small variation in exhumation estimates by both techniques is expected for areas where the interested unconformity is not at the present-day ground level. This is because subsequent sediment loading reduces the gross exhumation, which is the vertical displacement between the reference curve and the anomalous curve (depth of the sample) at the time of exhumation. (Corcoran and Doré, 2005; Hillis, 1995). As a result, the present estimated exhumation magnitude using the compaction method which is represented by the difference between the reference curve and present-day depth of the sample is reduced by an amount that is equal to the post exhumation reburial (Corcoran and Doré, 2005; Hillis, 1995). Thus, the magnitude of estimated exhumation using the compaction method represents minimum estimates as opposed to the total amount of exhumation that occurred at the time of denudation (Corcoran and Doré, 2005; Hillis, 1995; Licciardi et al., 2020).This reduction in the amount of exhumation is termed apparent exhumation by Hillis (1995) and net exhumation by Corcoran and Doré (2005) and Licciardi et al., (2020). The amount of post-exhumation reburial may vary across the basin as it depends on loading factors such as the volume and density of overlying sediments (Allen and Allen, 2013). These factors may vary across the basin and explain the small variation in exhumation estimates obtained by both methods for wells in the western part of the basin.

On the other hand, in areas where the thermal method (VR) estimated anomalously high exhumation magnitudes, compared to the compaction method for the same well location, VR oxidation effects (Hillis, 1995) or localised heating bodies such as hot fluids or intrusives accounted for higher VR values (Dow, 1977; Duddy et al., 1994) and the higher exhumation estimates associated with the thermal (VR) method. VR data quality including oxidation effects are not considered as they may be difficult to recognise in secondary VR data. Although igneous intrusives have not been reported in the Kidson Sub-basin, they have been reported in other parts of the Canning Basin including Fitzroy Trough and Lennard Shelf (Arne et al., 1989; Hashimoto et al., 2018). Also, sediment hosted base metal deposits as well as uranium deposits have been reported in the Canning Basin (Botten, 1984; Mccracken et al., 1997; Veamcombe et al., 1995). These deposits are associated with hot hydrothermal fluid circulation (Hoggard et al., 2020). Although external heating bodies such as hydrothermal fluids and igneous intrusives may influence porosity of the surrounding sediments, VR are more susceptible to variations in temperature (Johnson et al., 2017; Makuluni et al., 2021). Thus, the occurrence of anomalous high temperature measurements and associated high exhumation magnitudes estimated by the thermal (VR) method and the wide variation in exhumation estimates between both techniques obtained from wells in the eastern part of the Kidson Sub-basin strongly suggest that temperature signatures of sediments in the eastern part of the basin have been influenced by localised heating bodies. As a result, these anomalous high exhumation estimates obtained by the thermal technique for wells in the eastern part of the Kidson Sub-basin are over-estimated. Exhumation magnitudes estimated by the compaction method have therefore been used for further analysis and discussion.

5.2 Temperature profiles and geothermal gradients in the Kidson Sub-basin.

Comparison of the paleo-temperature profile with the present-day temperature profile at the various well locations indicate that sediments were hotter in the past than predicted for the depth the sediments are presently at. This is shown by the offset of the paleo-temperature profiles to higher temperatures (Fig. 8). Temperatures during the paleo-thermal maximum in the Late Triassic were significantly higher than the present day. Temperatures have decreased by 40 to 80^0C from the Late Triassic to the present-day across the Kidson Sub-basin (Fig. 8). At all the well locations, except Sahara-1, the paleo-temperature profiles are sub-parallel to the present-day temperature profiles and geothermal gradients range between 28 to 37^0C/km (Fig. 8). At these well locations, the paleo-geothermal gradients are 0.4 to 5.7^0C/km higher than the present-day geothermal gradient. On the contrary, the present-day and paleo temperature gradients at Sahara-1 are 44^0C/km and 64^0C/km, respectively. These are extremely high compared to other well locations. Moreover, the relationship between the present-day and paleo-temperature profiles suggest significant influence of increase in basal heat flow (Bray et al., 1992; O'Sullivan et al., 1995). However, the effects of basal heat flow are regional and affect larger areas (Allen and Allen, 2013). Thus, considering the proximity of Sahara-1 with other well locations, such large difference between present-day and paleo-temperature gradients, corresponding to large variation in basal heat flow would have been observed at other adjacent well locations. Moreover, typical present-day geothermal gradients reported in the Canning Basin are less than 43^0C/km (Horstman, 1984). These high geo-thermal gradients are only observed at one well location and suggest that the temperature data (BHT and VR) from Sahara-1 may have been significantly influenced by localised heating bodies, such as hot fluids associated with magmatic bodies, or the BHT and VR data may not be accurate. As a result, we do not consider the temperature data from Sahara-1 in the general temperature analysis of the Kidson Sub-basin.

The sub-parallel relationship between the present-day and paleo-temperature profiles, and associated small variation between the present-day and paleo- geothermal gradients observed at all the other well locations (Fig. 8) indicate that heating to maximum temperatures was predominantly due to deep burial (during the Late Triassic subsidence) with little contribution from increase in basal heat flow (Bray et al., 1992; O'Sullivan et al., 1995). Also, the sub-parallel present-day and paleo-temperature profiles (Fig. 8) demonstrate that cooling to present-day temperatures was predominantly due to exhumation (Bray et al., 1992; Green et al., 2002; O'Sullivan, 1999). Similar temperature profiles have been reported for White Hills-1 located within the Gregory Sub-basin (northeast Canning Basin), about 200 km from the Kidson Sub-basin (Duddy et al., 2003). Thus, our results agree with the work of Duddy et al. (2003) and we therefore conclude that maximum paleo-temperatures in the eastern Canning Basin, particularly the Kidson Sub-basin have been influenced by slight increase in basal heat flow. Timing constraints from burial history and apatite fission track analysis both indicate that maximum paleo-temperatures in the Kidson Sub-basin were attained in the Early Triassic (see section 5.1). Thus, we associate this slight increase in basal heat flow to the Late Carboniferous to Early Triassic extensional event (Point Moody Extension) that preceded the Jurassic Fitzroy

Transpressional Movement. During extension, heat flow is generally raised due to the upwelling of the hot asthenosphere beneath the stretched and thinned lithosphere (Allen and Allen, 2013; McKenzie, 1978; Waples, 2001). Heat flow may vary little or significantly long after the extensional event. As described above, the nearly parallel present-day and paleo-temperatures profiles and associated gradients indicate little variation in heat flow from the Late Triassic thermal maximum until the present-day.

Geothermal gradients within the Kidson Sub-basin are consistent with results from other parts of the Canning Basin, such as the Lennard Shelf and Fitzroy Trough (Arne et al., 1989; Horstman, 1984). Based on geothermal gradient, sedimentary basins have been classified into three broad categories including normal, hypothermal and hyperthermal basins (Allen and Allen, 2013; Robert, 1988). In general, present-day and paleo geothermal gradients in the Kidson Sub-basin range from 28 to 37^0C/km and are considered to fall within the normal to hyperthermal group of basins (Allen and Allen, 2013). The range of present-day and pale-geothermal gradients within the Kidson Sub-basins is consistent with the general classification of the basin as an intra-cratonic rift basin (Forman and Wales, 1981; Hashimoto et al., 2018; Hocking et al., 1994; Shaw et al., 1994).

5.3 Comparison of present study with earlier exhumation studies

The work of Kennard et al. (1994b) represents the only extensive exhumation studies within the Kidson Sub-basin. Their work involved the estimation of magnitude of exhumation through time using the WinBury 1.4 geohistorical analysis program. Their study used a wide range of paleo-thermal indicators including Vitrinite Reflectance (VR), Spore Colour Index (SCI), Conodont Colour Alteration Index (CAI =Ro equivalent), Thermal Alteration Index (TAI) and Tmax obtained from Rock-Eval Pyrolysis. However, minimum exhumation estimates from this study obtained using the compaction method (see 5.2 for discussion) during the various exhumation episodes are higher than estimates from Kennard et al. (1994b) (Table 6). Moreover, more recent studies from VR and apatite fission track analysis (AFTA) from other parts of the Canning Basin also indicate higher magnitude of exhumation during the Late Triassic-Early Jurassic period compared to Kennard's study. For example, Duddy et al. (2006) and Green (2014) concluded that between 800-2800 m (maximum likelihood estimate of 1300 m) and between 950-1950 m (maximum likelihood estimate 1400 m) of sediments were removed at Acacia-2 and McLarty-1, respectively during the Early Jurassic Exhumation period. However, Kennard et al. (1994b) estimated 400 m and 450 m of uplift and erosion at those well locations.

We have not investigated the accuracy and limitations of WinBury 1.4 geohistorical analysis program. However, major possible sources of error in exhumation estimates by Kennard et al. (1994b) come from their approach in the use of paleo-thermal data. In their study, paleo-thermal data at individual well locations were divided into 3 sections with the assumption that peak paleo temperatures were attained at three different periods corresponding to major extension events in the Kidson Sub-basin. Thus, paleo-thermal data obtained from sediments deposited during a particular heating episode were used to estimate the amount of exhumation during the following inversion episode. For example, paleo-thermal data from Ordovician to

Early Silurian sediments were assumed to represent the paleo-thermal maximum during the Ordovician to Silurian extension and heating episode. These were used to estimate the amount of exhumation during the succeeding inversion episode in the Late Silurian-Early Devonian period. Similar approach was employed to estimate the magnitude of exhumation during other inversion episodes. Thus, a major limitation with their approach was the division of paleo-thermal data from individual wells into segments, which were not constrained by required timing information. Instead, the division was based on the timing of extension and associated subsidence with the assumption that each extension episode corresponded to maximum heating. Applying the methodology and constraints used in this study to raw paleo-thermal data obtained from the work of Kennard et al. (1994b) would provide a more suitable basis for comparison of results as minor errors that may be associated with variation in data will be eliminated. However, raw paleo-thermal data employed by Kennard et al. (1994b) were not available for such analysis and comparison.

Table 6. Comparison of the magnitude of exhumation estimated by Kennard et al. (1994b) and this study

Well Name	**Early Jurassic (Fitzroy Transpression)**			**Mid Carboniferous (Meda Transpression)**		**Early Devonian (Prices Creek Compression)**	
	This study[1]	Combined Kennard et al. (1994b)[2]	Kennard et al. (1994b)	This study[1]	Kennard et al. (1994b)	This study[1]	Kennard et al. (1994b)
Kidson 1	800	700	400	500	300	350	0
Wilson Cliffs 1	700	420	250	600	150	350	20
Frankenstein 1	1100	550	450	700	100	450	0
Sahara 1	950	650	400	750	250	500	0

[1]Estimated magnitude of exhumation presented in this table represent minimum estimates obtained from the compaction method (see section 5.2 for discussion).
[2]Combined estimate of Kennard et al. (1994b) if all exhumation is placed in the Early Jurassic instead of across the three time periods.

Previously published apatite fission track analysis (AFTA) and corresponding thermal history modelling from Duddy et al. (2006, 2003) and Green (2014) indicate three main cooling events in the Kidson Sub-basin, with the most prominent occurring in the Late Triassic. These constraints imply that maximum heating in the Kidson Sub-basin was likely attained during the Early Triassic extension period prior to the development of the Fitzroy Transpression (Fig. 3; Cadman et al., 1993; Forman and Wales, 1981; Hashimoto et al., 2018; Parra-Garcia et al., 2014; Shaw et al., 1994; Zhan and Mory, 2013). These results indicate the at the this event is likely the regional Mesozoic erosional unconformity, U_2, observed on seismic profiles that extends across the entire Kidson Sub-basin (Fig. 7) and which has been reported in other parts of the Canning Basin (Hashimoto et al., 2018).

In this instance, previous heating and thermal records were overridden by the thermal event of the Early Triassic. This implies that the entire paleo-thermal data (VR, CAI, TAI, SCI) obtained from stratigraphic units at the individual well locations employed by Kennard et al. (1994b) corresponds to a single and uniform heating episode associated with the Early Triassic heating episode. It also means that obtained VR paleo-thermal data are only appropriate for estimating the magnitude of exhumation during the cooling and exhumation period in the Early Jurassic which immediately followed the paleo-thermal maximum (Corcoran and Doré, 2005). Thus, the separation of paleo-thermal data into distinct thermal episodes may contribute to the very low exhumation estimates in the Kidson Sub-basin during the various inversion episodes as employed by Kennard et al. (1994b). Using the compaction method in combination with the estimates from the VR method, allows for the minimum exhumation to be better estimated across the 3 different time periods and Kennard et al.(1994b)'s results are closer to ours for the Early Triassic if combined as shown in Table 6.

5.4 Implication of Exhumation Magnitudes on the Tectonic Evolution of the Kidson Sub-basin.

The magnitude and distribution of exhumation in a terrane during an inversion episode are affected by two main mechanical factors demonstrated by theoretical studies (Cloetingh and Ziegler, 2007; Turner and Williams, 2004; Ziegler et al., 1995), numerical, experimental and analogue models (Casas et al., 2001; Cerca et al., 2010; Cloetingh et al., 2008, 2005; Dooley and Schreurs, 2012; Schellart and Strak, 2016). These factors include the variation in rheology of the basement units and the compressive stresses applied. Since the development of the Kidson Sub-basin is associated with the overall development of the Canning Basin, results from the Kidson Sub-basin alone may not be enough to explain the variation in exhumation magnitudes with space and time within the sub-basin.

The rheological strength of the basement unit underlying the Canning Basin is considered to increase from northwest to southeast, with the south-eastern parts of the Kidson Sub-basin been the strongest (Connors et al., 2018). The Meda Transpression, the Prices Creek and Fitzroy inversional episodes shows a decrease in exhumation from northwest to southeast across the Sub-basin (Fig. 12). This suggest that areas with relative basement weaknesses experienced higher magnitudes of exhumation. This result is consistent with analogue models which indicate that the effects of compressional stress are intensified in areas of weak basement units (Dooley and Schreurs, 2012; Schellart and Strak, 2016). Thus, the spatial distribution of exhumation in the Kidson Sub-basin may be attributed to variation or heterogeneity in basement units underlying the Kidson Sub-basin.

Our results indicate a noticeable progressive increase in the magnitude of exhumation with time, with the lowest exhumation magnitudes recorded during the earliest inversion episode (the late Silurian to Early Devonian Prices Creek Compression), medium exhumation estimates recorded during the second inversion episode (the middle Carboniferous Meda Transpression) and highest exhumation magnitudes recorded during the latest inversion period (the Early Jurassic Fitzroy Transpression) (Fig. 12 A1, B and C; Table 5). Although data was not available to constrain the amount of exhumation during subsequent inversion episodes which occurred in the Cretaceous and Cenozoic (Fig. 3), these exhumation events are considered to have

minimal effects in the basin compared to the Late Triassic-Early Jurassic exhumation episode (Duddy et al., 2003, 2006; Hashimoto et al., 2018; Shaw et al.,1994).

There is no available data to compare the intensity of compressive stresses that reached the Kidson Sub-basin during the various compressional episodes. However, it is likely that the compressional stresses were far greater during the Meda Transpression and Prices Creek compression, since these events are associate with the major Alice Springs Orogenic event and Gondwana-Laurassia collision, as mentioned previously (Klootwijk, 2013; Li and Powell, 2001). The likely decreasing intensity of compressional stresses is in contrast to the increase in exhumation until the Cenozoic, but it is likely that the Canning Basin experienced progressive weakening of the basement units from the series of compressions (Shaw et al., 1994). While the significant decrease in effects of exhumation during the Cretaceous and Cenozoic indicate a probable significant decrease in the intensity of compressional stress during these inversional episodes.

6. Summary and Conclusion

In this study, we investigated the amount of exhumation during major inversion episodes in the Kidson Sub-basin by integrating a wide range of data set including seismic, stratigraphic, core well-log and thermal data. These inversion episodes are the Prices Creek Compression (middle Silurian to Early Devonian), the Meda Transpression (middle Carboniferous to Early Devonian), and the Fitzroy Transpression (Late Triassic to Early Jurassic).

Two independent methods, namely, thermal and compaction techniques were employed to estimate the magnitude of exhumation during these three major inversion episodes. These independent methods both provide important constraints on results. Results indicate that at least 300-500 m of exhumation occurred during the Prices Creek Compression, 500 to 750 m of exhumation occurred during the Meda Transpression and 800 to 1200 m of exhumation occurred during the Fitzroy Transpression. Integration of timing constraints from AFTA and burial history analysis indicate the VR obtained at the individual well location represent a single and uniform heating episode during the Early Triassic. Results indicate that thermal signatures of sediments in the eastern part of the sub-basin have been influenced by hot fluids associated with magmatism. For all the three major inversion episodes, our study indicates that the magnitudes of exhumation are higher than previously thought. Exhumation in all three episodes decreases from northwest to southeast, likely due to increased crustal strength in that direction.

Acknowledgements

The authors acknowledge Tehani Palu for her valuable comments and insights in the manuscript as well as Peter Japsen and the anonymous reviewers for their insightful comments. George Marfo and Stuart Clark acknowledge DUG Technology Ltd. for the use of DUG Insight software.

References

Allen, P.A., Allen, J.R., 2013. Basin analysis: Principles and Application to Petroleum Play Assessment, Third edition. ed. John Wiley & Sons, Chichester, West Susex, UK.

Arne, D.C., Green, P.F., Duddy, I.R., Gleadow, A.J.W., Lambert, I.B., Lovering, J.F., 1989. Regional thermal history of the Lennard shelf, Canning Basin, from apatite fission track analysis: Implications for the formation of Pb-Zn ore deposits. Australian Journal of Earth Sciences 36, 495–513. https://doi.org/10.1080/08120098908729506

Athy, L.F., 1930. Density, Porosity, and Compaction of Sedimentary Rocks. AAPG Bulletin 14, 1–24. https://doi.org/10.1306/3D93289E-16B1-11D7-8645000102C1865D

Barker, C.E., Pawlewicz, M.J., 1994. Calculation of Vitrinite Reflectance from Thermal Histories and Peak Temperatures, in: Mukhopadhyay, P.K., Dow, W.G. (Eds.), Vitrinite Reflectance as a Maturity Parameter, ACS Symposium Eries. American Chemical Society, Washington DC, p. 14.

Betts, P.G., Giles, D., Lister, G.S., Frick, L.R., 2002. Evolution of the Australian lithosphere. Australian Journal of Earth Sciences 49, 661–695. https://doi.org/10.1046/j.1440-0952.2002.00948.x

Botten, P., 1984. Uranium exploration in the Canning Basin: a case study., in: Purcell, P.G. (Ed.), The Canning Basin W.A, GSA/PESA Canning Basin Symposium Perth. Petroleum Exploration Society of Australia (WA Branch), Perth.

Bradshaw, M., Borissova, I., Edwards, D.S., Gibson, G.M., Hashimoto, T., Nelson, G.J., Totterdell, J.M., 2012. Chapter 4: Out of Gondwana. Shaping a nation: a geology of Australia, in: Shaping a Nation: Geology of Australia. ANU Press.

Bray, R.J., Green, P.F., Duddy, I.R., 1992. Thermal history reconstruction using apatite fission track analysis and vitrinite reflectance: a case study from the UK East Midlands and Southern North Sea. Geological Society, London, Special Publications 67, 3–25. https://doi.org/10.1144/GSL.SP.1992.067.01.01

Cadman, S.J., Pain, L., Vuckovic, V., Le Poidevin, R.R. (Eds.), 1993. Canning Basin, W. A, Australian petroleum accumulations report. Bureau of Resource Sciences, Canberra.

Carlsen, G.M., Ghori, K.A.R., 2005. Canning Basin and Global Palaeozoic Petroleum Systems-A Review. The APPEA Journal 45, 349. https://doi.org/10.1071/AJ04028

Casas, A.M., Gapais, D., Nalpas, T., Besnard, K., Román-Berdiel, T., 2001. Analogue models of transpressive systems. Journal of Structural Geology 23, 733–743. https://doi.org/10.1016/S0191-8141(00)00153-X

Cerca, M., Ferrari, L., Corti, G., Bonini, M., Manetti, P., 2010. Analogue model of inversion tectonics explaining the structural diversity of Late Cretaceous shortening in southwestern Mexico. Lithosphere 2, 172–187. https://doi.org/10.1130/L48.1

Cloetingh, S., Beekman, F., Ziegler, P.A., Wees, J.-D.V., Sokoutis, D., 2008. Post-rift compressional reactivation potential of passive margins and extensional basins. https://doi.org/10.1144/SP306.2

Cloetingh, S., Matenco, L., Bada, G., Dinu, C., Mocanu, V., 2005. The evolution of the Carpathians-Pannonian system: Interaction between neotectonics, deep structure, polyphase orogeny and sedimentary basins in a source to sink natural laboratory. Tectonophysics 410, 1–14. https://doi.org/10.1016/j.tecto.2005.08.014

Cloetingh, S., Ziegler, P.A., 2007. 6.11 - Tectonic Models for the Evolution of Sedimentary Basins, in: Schubert, G. (Ed.), Treatise on Geophysics. Elsevier, Amsterdam, pp. 485–611. https://doi.org/10.1016/B978-044452748-6.00109-7

Command Petroleum NL, 1989. Frankenstein 1 final well completion report (No. EP 232). Command Petroleum NL, Australia.

Connors, K., Jorand, C., Haines, P., Zhan, Y., Pryer, L., 2018. Uncovering the Canning Basin: a new comprehensive SEEBASE® model. The APPEA Journal 58, 793. https://doi.org/10.1071/AJ17073

Corcoran, D., Clayton, G., 1999. INTERPRETATION OF VITRINITE REFLECTANCE PROFILES IN THE CENTRAL IRISH SEA AREA: IMPLICATIONS FOR THE TIMING OF ORGANIC MATURATION. J Petroleum Geol 22, 261–286. https://doi.org/10.1111/j.1747-5457.1999.tb00987.x

Corcoran, D.V., Clayton, G., 2001. Interpretation of vitrinite reflectance profiles in sedimentary basins, onshore and offshore Ireland. Geological Society, London, Special Publications 188, 61–90. https://doi.org/10.1144/GSL.SP.2001.188.01.04

Corcoran, D.V., Doré, A.G., 2005. A review of techniques for the estimation of magnitude and timing of exhumation in offshore basins. Earth-Science Reviews 72, 129–168. https://doi.org/10.1016/j.earscirev.2005.05.003

Cox, D.P., Lindsey, D.A., Singer, D.A., Moring, B.C., Diggles, M.F., 2003. Sediment-Hosted Copper Deposits of the World: Deposit Models and Database (Open-File Report), Open-File Report. United States Geological Survey, Denver, Colorado.

Crain, E.R., 2002. Crain's petrophysical handbook. Spectrum 2000 Mindware Limited.

Dentith, M., 2012. Estimating the amount of uplift during Canning Basin tectonic events using well logs. ASEG Extended Abstracts 2012, 1–3. https://doi.org/10.1071/ASEG2012ab074

Dooley, T.P., Schreurs, G., 2012. Analogue modelling of intraplate strike-slip tectonics: A review and new experimental results. Tectonophysics 574–575, 1–71. https://doi.org/10.1016/j.tecto.2012.05.030

Doreʹ, A.G., Corcoran, D.V., Scotchman, I.C., 2002. Prediction of the hydrocarbon system in exhumed basins and application to the NW European margin., in: Doré, A.G., Cartwright, J.A., Stoker, M.S., Turner, J.P., White, N. (Eds.), Exhumation of the North Atlantic Margin: Timing, Mechanisms and Implications for Petroleum Exploration, Geological Society, London, Special Publications. pp. 401–429.

Dow, W.G., 1977. Kerogen studies and geological interpretations. Journal of Geochemical Exploration 7, 79–99. https://doi.org/10.1016/0375-6742(77)90078-4

Duddy, I.R., Erout, B., 2001. AFTA calibrated 2-D modelling of hydrocarbon generation and migration using Temispack: Preliminary results from the Otway Basin, in: Hill, P.J., Bernecker, T. (Eds.), Eastern Australia Basins Symposium, A Refocussed Energy Perspective for the Future. pp. 485–497.

Duddy, I.R., Green, P.F., Bray, R.J., Hegarty, K.A., 1994. Recognition of the thermal effects of fluid flow in sedimentary basins. Geological Society, London, Special Publications 78, 325. https://doi.org/10.1144/GSL.SP.1994.078.01.22

Duddy, I.R., Green, P.F., Gibson, H.J., Hegarty, K.A., 2003. Regional palaeo-thermal episodes in northern Australia, in: Proceedings of the Timor Sea Symposium. Presented at the Timor Sea Petroleum Geoscience, Timor Sea Petroleum Geoscience, Darwin Northern Territory, p. 20.

Duddy, I.R., Moore, M.E., O'Brien, C., 2006. Thermal History Reconstruction in Five Canning Basin Wells: Acacia-1 &-2, Kidson-1, Willara-1 & Yulleroo-1 Based on Apatite Fission Track Analysis (AFTA®) and Vitrinite Reflectance Data. Geotrack Report, Victoria, Australia.

Edgoose, C.J., 2012. The Amadeus Basin, central Australia. Episodes Journal of International Geoscience 35, 256–263. https://doi.org/10.18814/epiiugs/2012/v35i1/025

Forman, D.J., Wales, D.W., 1981. Geological evolution of the Canning Basin, Western Australia. Australian Govt. Pub. Service, Canberra.

Gallagher, K., 2012. Uplift, denudation, and their causes and constraints over geological timescales, in: Phanerozoic Regional Geology of the World. Elsevier, pp. 608–644. https://doi.org/10.1016/B978-0-444-53042-4.00022-4

Geoscience Australia, 2020. Kidson Sub-Basin Prospectivity [WWW Document]. URL https://www.ga.gov.au/eftf/data-and-publications/case-studies/latest-case-studies/kidson-sub-basin-prospectivity (accessed 10.19.21).

Ghori, K.A.R., 2013. Petroleum geochemistry and petroleum systems modelling of the Canning Basin, Western Australia (No. 124). Geological Survey of Western Australia.

Green, P.F., 2014. Thermal history reconstruction in Canning Basin Wells Nicolay-1, Gibb Maitland-1, and Mclarty-1 based on AFTA and organic maturity data. Geotrack Report Number 1148 (No. 1148). Geotrack International Pty Ltd, Victoria, Australia.

Green, P.F., Duddy, I.R., Hegarty, K.A., 2002. Quantifying exhumation from apatite fission-track analysis and vitrinite reflectance data: precision, accuracy and latest results from the Atlantic margin of NW Europe. Geological Society, London, Special Publications 196, 331–354.

Haines, P.W., Hand, M., Sandiford, M., 2001. Palaeozoic synorogenic sedimentation in central and northern Australia: A review of distribution and timing with implications for the evolution of intracontinental orogens. Australian Journal of Earth Sciences 48, 911–928. https://doi.org/10.1046/j.1440-0952.2001.00909.x

Haines, P.W., Wingate, M.T.D., 2007. Contrasting depositional histories, detrital zircon provenance and hydrocarbon systems: did the Larapintine Seaway link the Canning and Amadeus basins during the Ordovician, in: Proceedings Central Australian Basin Symposium, Special Publications. pp. 36–51.

Haines, P.W., Wingate, M.T.D., Kirkland, C.L., 2013. Detrital Zircon U–Pb Ages from the Paleozoic of the Canning and Officer Basins, Western Australia: Implications for Provenance and Interbasin Connections 20.

Hand, M., Sandiford, M., 1999. Intraplate deformation in central Australia, the link between subsidence and fault reactivation. Tectonophysics 305, 121–140. https://doi.org/10.1016/S0040-1951(99)00009-8

Hashimoto, T., Bailey, A., Chirinos, A., Carr, L.K., 2018a. Onshore basin inventory volume 2: the Canning, Perth and Officer basins. Geoscience Australia. https://doi.org/10.11636/Record.2018.018

Hashimoto, T., Bailey, A., Chirinos, A., Carr, L.K., 2018b. Onshore basin inventory volume 2: the Canning, Perth and Officer basins. Geoscience Australia. https://doi.org/10.11636/Record.2018.018

Hillis, R.R., 1995. Regional Tertiary Exhumation in and around the United Kingdom. Geological Society, London, Special Publications 88, 167–190. https://doi.org/10.1144/GSL.SP.1995.088.01.11

Hocking, R.M., Mory, A.J., Williams, I.R., 1994. An Atlas of Neoproterozoic and Phanerozoic Basins of Western Australia., in: The Sedimentary Basins of Western Australia: Proceedings of Petroleum Exploration Society of Australia Symposium, Perth. pp. 21–43.

Hoggard, M.J., Czarnota, K., Richards, F.D., Huston, D.L., Jaques, A.L., Ghelichkhan, S., 2020. Global distribution of sediment-hosted metals controlled by craton edge stability. Nat. Geosci. 13, 504–510. https://doi.org/10.1038/s41561-020-0593-2

Horstman, E.L., 1984. Evidence for Post-Permian Epeirogenic Uplift in the Canning Basin from Vitrinite Reflectance Data, in: Purcell, P.G. (Ed.), The Canning Basin, W.A. Geological Soceity of Australia and Petroleum Exploration Society of Australia, p. 9.

Japsen, P., 2000. Investigation of multi-phase erosion using reconstructed shale trends based on sonic data. Sole Pit axis, North Sea. Global and Planetary Change 24, 189–210. https://doi.org/10.1016/S0921-8181(00)00008-4

Jensen, L.N., Schmidt, B.J., 1993. Neogene Uplift and Erosion Offshore South Norway: Magnitude and Consequences for Hydrocarbon Exploration in the Farsund Basin, in: Spencer, A.M. (Ed.), Generation, Accumulation and Production of Europe's Hydrocarbons III. Springer Berlin Heidelberg, Berlin, Heidelberg, pp. 79–88. https://doi.org/10.1007/978-3-642-77859-9_7

Johnson, L.M., Rezaee, R., Kadkhodaie, A., Smith, G., Yu, H., 2017. A new approach for estimating the amount of eroded sediments, a case study from the Canning Basin, Western Australia. Journal of Petroleum Science and Engineering 156, 19–28. https://doi.org/10.1016/j.petrol.2017.05.008

Keep, M., Harrowfield, M., Crowe, W., 2007. The Neogene tectonic history of the North West Shelf, Australia. Exploration Geophysics 38, 151–174. https://doi.org/10.1071/EG07022

Kennard, J.M., Jackson, M.J., Romine, K.K., Shaw, R.D., Southgate, P.N., 1994a. Depositional Sequences and Associated Petroleum Systems of the Canning Basin, WA, in: Purcell, P.G., Purcell, R.R. (Eds.), The Sedimentary Basins of Western Australia. Proceedings of the Petroleum Exploration Society of Australia Symposium, Perth. pp. 657–676.

Kennard, J.M., Jackson, M.J., Romine, K.K., Southgate, P.N., 1994b. Canning Basin Project stage II - geohistory modelling. Australian Geological Survey Organisation, Canberra.

Kesler, S.E., Wilkinson, B.H., 2006. THE ROLE OF EXHUMATION IN THE TEMPORAL DISTRIBUTION OF ORE DEPOSITS. Economic Geology 101, 919–922. https://doi.org/10.2113/gsecongeo.101.5.919

Klootwijk, C., 2013. Middle–Late Paleozoic Australia–Asia convergence and tectonic extrusion of Australia. Gondwana Research 24, 5–54. https://doi.org/10.1016/j.gr.2012.10.007

Li, Z.X., Powell, C.McA., 2001. An outline of the palaeogeographic evolution of the Australasian region since the beginning of the Neoproterozoic. Earth-Science Reviews 53, 237–277. https://doi.org/10.1016/S0012-8252(00)00021-0

Licciardi, A., Gallagher, K., Clark, S.A., 2020. Estimating uncertainties on net erosion from well-log porosity data. Basin Res 32, 51–67. https://doi.org/10.1111/bre.12366

Lord, A.S., Kobos, P.H., Borns, D.J., 2014. Geologic storage of hydrogen: Scaling up to meet city transportation demands. International Journal of Hydrogen Energy 39, 15570–15582. https://doi.org/10.1016/j.ijhydene.2014.07.121

Luo, Q., Fariborz, G., Zhong, N., Wang, Y., Qiu, N., Skovsted, C.B., Suchý, V., Hemmingsen Schovsbo, N., Morga, R., Xu, Y., Hao, J., Liu, A., Wu, Jin, Cao, W., Min, X., Wu, Jia, 2020. Graptolites as fossil geothermometers and source material of hydrocarbons: An overview of four decades of progress. Earth-Science Reviews 200, 103000. https://doi.org/10.1016/j.earscirev.2019.103000

MacNeill, M., Marshall, N., McNamara, C., 2018. New Insights into a major Early-Middle Triassic Rift Episode in the NW Shelf of Australia. ASEG Extended Abstracts 2018, 1–5. https://doi.org/10.1071/ASEG2018abM3_3B

Magara, K., 1980. Comparison of porosity-depth relationships of shale and sandstone. Journal of Petroleum Geology 3, 175–185. https://doi.org/10.1111/j.1747-5457.1980.tb00981.x

Makuluni, P., Johnson, L.M., Hauser, J., Langhi, L., Clark, S., 2021. Quantifying exhumation using compaction and vitrinite reflectance in the Southern Bonaparte Basin, North West Shelf, Australia. Marine and Petroleum Geology 134, 105318. https://doi.org/10.1016/j.marpetgeo.2021.105318

Mccracken, S.R., Etminan, H., Connor, A.G., Williams, V.A., 1997. Geology of the Admiral Bay carbonate-hosted zinc-lead deposit, Canning Basin, Western Australia, in: Sabgster, S.F. (Ed.), Carbibate-Hosted Lead-Zinc Deposits. Society of Economic Geologists, El Pasco, Texas, pp. 330–349.

McKenzie, D., 1978. Some remarks on the development of sedimentary basins. Earth and Planetary Science Letters 40, 25–32. https://doi.org/10.1016/0012-821X(78)90071-7

Munroe, S., Ham, A., Griffin, S., 2004. Amadeus Basin SEEBASE project: September 2004 (No. Record 2004-010). Northern Territory Geological Survey.

O'Sullivan, 1999. Thermochronology, denudation and variations in palaeosurface temperature: a case study from the North Slope foreland basin, Alaska: Denudation/cooling of the North Slope foreland basin. Basin Research 11, 191–204. https://doi.org/10.1046/j.1365-2117.1999.00094.x

O'Sullivan, P.B., Hanks, C.L., Wallace, W.K., Green, P.F., 1995. Multiple episodes of Cenozoic denudation in the northeastern Brooks Range: fission-track data from the Okpilak batholith, Alaska 32, 13.

Parra-Garcia, M., Sanchez, G., Dentith, M., George, A.D., 2014. Regional structural and stratigraphic study of the Canning Basin, Western Australia. Geological Survey of Western Australia Report 140, 215.

Passmore, V., Towner, R., 1987. A History of Geological Exploration in the Canning Basin, Western Australia. Earth Sciences History 6, 159–177. https://doi.org/10.17704/eshi.6.2.jm774585j6382583

Reeckmann, S.A., Mebberson, A.J., 1984. Igneous. Intrusions in the North-West Canning Basin and their Impact on Oil Exploration, in: Purcell, P.G. (Ed.), The Canning Basin W.A, GSA/PESA Canning Basin Symposium Perth. Petroleum Exploration Society of Australia (WA Branch), Perth.

Ringrose, C.R., 1984. The Geology and Genesis of the Narlarla Lead-Zinc Deposits, Napier Range, W.A. PESA - Petroleum Exploration Society of Australia.

Robert, P., 1988. Organic metamorphism and geothermal history: microscopic study of organic matter and thermal evolution of sedimentary basins. Springer.

Schellart, W.P., Strak, V., 2016. A review of analogue modelling of geodynamic processes: Approaches, scaling, materials and quantification, with an application to subduction experiments. Journal of Geodynamics 100, 7–32. https://doi.org/10.1016/j.jog.2016.03.009

Sclater, J.G., Christie, P.A.F., 1980. Continental stretching: An explanation of the Post-Mid-Cretaceous subsidence of the central North Sea Basin. J. Geophys. Res. 85, 3711–3739. https://doi.org/10.1029/JB085iB07p03711

Shaw, R.D., Sexton, M.J., Zeilinger, I., 1994. The tectonic framework of the Canning Basin, WA, including 1:2 million structural elements map of the Canning Basin. Australian Geological Survey Organisation, Canberra City.

Southby, C., Carr, L., Henson, P., Haines, P., Zhan, A., Anderson, J., MacFarlane, S., Fomin, T., Costelloe, R., 2019. Exploring for the future: Kidson Sub-basin seismic interpretation. ASEG Extended Abstracts 2019, 1–3. https://doi.org/10.1080/22020586.2019.12073007

Sweeney, J.J., Burnham, A.K., 1990. Evaluation of a Simple Model of Vitrinite Reflectance Based on Chemical Kinetics (1). Bulletin 74. https://doi.org/10.1306/0C9B251F-1710-11D7-8645000102C1865D

Tassone, D.R., Holford, S.P., Duddy, I.R., Green, P.F., Hillis, R.R., 2014. Quantifying Cretaceous–Cenozoic exhumation in the Otway Basin, southeastern Australia, using sonic transit time data: Implications for conventional and unconventional hydrocarbon prospectivity. Bulletin 98, 67–117. https://doi.org/10.1306/04011312111

Turner, J.P., Williams, G.A., 2004. Sedimentary basin inversion and intra-plate shortening. Earth-Science Reviews 65, 277–304. https://doi.org/10.1016/j.earscirev.2003.10.002

U.S.A Energy Information Administration, U.S.A.D. of E., 2013. Technically Recoverable Shale Oil and Shale Gas Resources: An Assessment of 137 Shale Formations in 41 Countries Outside the United States. Washington DC.

U.S.A Energy Information Administration, U.S.A.D. of E., 2011. World Shale Gas Resources: An Initial Assessment of 14 Regions Outside the United States. Washington DC.

Veamcombe, J.R., Dörling, S.L., Dentith, M.C., Chisnall, A.W., Christensen, J.N., McNaughton, N.J., Playford, P.E., Rayner, M.J., Reed, A.R., 1995. Zinc-Lead Mineralization on the Southeast Lennard Shelf, Canning Basin, Western Australia. https://doi.org/10.5382/GB.23

Waples, D.W., 2001. A New Model for Heat Flow in Extensional Basins: Radiogenic Heat, Asthenospheric Heat, and the McKenzie Model. Natural Resources Research 10, 227–238. https://doi.org/10.1023/A:1012521309181

Western Australia Department of Mines and Petroleum, G. of W.A., 2021. Canning Basin [WWW Document]. Department of Mines, Industry Regulation and Safety. URL https://www.dmp.wa.gov.au/Petroleum/Canning-Basin-10989.aspx (accessed 10.19.21).

Western Australia Department of Mines and Petroleum, G. of W.A., 2014. Western Australia's Petroleum and Geothermal Explorer's Guide, 2014 Edition. ed. Perth, WA.

Wyllie, M.R.J., Gregory, A.R., Gardner, L.W., 1956. ELASTIC WAVE VELOCITIES IN HETEROGENEOUS AND POROUS MEDIA. GEOPHYSICS 21, 41–70. https://doi.org/10.1190/1.1438217

Yamamoto, Y., Mukoyoshi, H., Ogawa, Y., 2005. Structural characteristics of shallowly buried accretionary prism: Rapidly uplifted Neogene accreted sediments on the Miura-Boso Peninsula, central Japan: STRUCTURES OF SHALLOW ACCRETIONARY PRISM. Tectonics 24, n/a-n/a. https://doi.org/10.1029/2005TC001823

Yule, C., Daniell, J., 2019. New insights into the offshore Canning Basin using a seamless onshore/offshore stratigraphic model. ASEG Extended Abstracts 2019, 1–5. https://doi.org/10.1080/22020586.2019.12073038

Zhan, Y., 2019. Seismic interpretation of salt occurrences in the southern Canning Basin, Western Australia. salt tectonics 15.

Zhan, Y., Mory, A.J., 2013. Structural Interpretation of the Northern Canning Basin, Western Australia 19.

Zhu, C., Qiu, N., Liu, Y., Xiao, Y., Hu, S., 2019. Constraining the denudation process in the eastern Sichuan Basin, China using low-temperature thermochronology and vitrinite reflectance data. Geological Journal 54, 426–437. https://doi.org/10.1002/gj.3191

Ziegler, P.A., Cloetingh, S., van Wees, J.-D., 1995. Dynamics of intra-plate compressional deformation: the Alpine foreland and other examples. Tectonophysics 252, 7–59. https://doi.org/10.1016/0040-1951(95)00102-6

Supplementary Files

This is a list of supplementary files associated with this preprint. Click to download.

- GraphicalAbstract.png